Theor. Comput. Fluid Dyn. (2006) 20: 377–404
DOI 10.1007/s00162-006-0014-1

ORIGINAL ARTICLE

Samuel N. Stechmann · Andrew J. Majda

The structure of precipitation fronts for finite relaxation time

Received: 13 July 2005 / Accepted: 31 January 2006 / Published online: 21 June 2006

Abstract When convection is parameterized in an atmospheric circulation model, what types of waves are supported by the parameterization? Several studies have addressed this question by finding the linear waves of simplified tropical climate models with convective parameterizations. In this paper's simplified tropical climate model, convection is parameterized by a nonlinear precipitation term, and the nonlinearity gives rise to precipitation front solutions. Precipitation fronts are solutions where the spatial domain is divided into two regions, and the precipitation (and other model variables) changes abruptly at the boundary of the two regions. In one region the water vapor is below saturation and there is no precipitation, and in the other region the water vapor is above saturation level and precipitation is nonzero. The boundary between the two regions is a free boundary that moves at a constant speed. It is shown that only certain front speeds are allowed. The three types of fronts that exist for this model are drying fronts, slow moistening fronts, and fast moistening fronts. Both types of moistening fronts violate Lax's stability criterion, but they are robustly realizable in numerical experiments that use finite relaxation times. Remarkably, here it is shown that all three types of fronts are robustly realizable analytically for finite relaxation time. All three types of fronts may be physically unreasonable if the front spans an unrealistically large physical distance; this depends on various model parameters, which are investigated below. From the viewpoint of applied mathematics, these model equations exhibit novel phenomena as well as features in common with the established applied mathematical theories of relaxation limits for conservation laws and waves in reacting gas flows.

Keywords Tropical atmospheric dynamics · Tropical convection · Moisture · Nonlinear relaxation equations · Hyperbolic free boundary problems

PACS 92.60.Ox · 92.60.Jq

1 Introduction

1.1 Background

Water vapor plays a major role in determining the earth's climate because there is a large release of latent energy when water vapor condenses. Phase changes of water are prominent in large, precipitating, convective

Communicated by R. Klein

S. N. Stechmann (✉) · A. J. Majda
Department of Mathematics and Center for Atmosphere Ocean Science, Courant Institute of Mathematical Sciences, New York University, 251 Mercer Street, New York, NY 10012, USA
E-mail: stechman@cims.nyu.edu

clouds, and energy from these phase changes can drive large-scale atmospheric motions. This link between precipitation and large-scale dynamics is seen in many parts of the earth's climate, such as El Niño/Southern Oscillation [38], the Hadley circulation [15], monsoons, the Madden–Julian Oscillation [24], and convectively-coupled equatorial waves [41–43]. These climatic events have a major impact on our ability to predict weather and climate not only in the tropics but also over the rest of the globe.

Arguably the most important type of convection in the tropical atmosphere is deep convection, which is characterized by towering clouds extending approximately 12–16 km in height from the boundary layer to the tropopause. Since more than half of total convective precipitation in the tropics is from deep convection [17], it is clear that deep convection plays an important role in tropical thermodynamics and therefore in the interaction between water vapor and large-scale dynamics. Global circulation models (GCMs), however, cannot resolve deep convective clouds because they typically have horizontal spatial scales of less than 50 km whereas grid spacings in GCMs are typically greater than 100 km. Therefore, instead of resolving deep convection, GCMs must parameterize it; that is, the energy changes associated with phase changes of water are parameterized in terms of large-scale variables. Such parameterizations are in need of improvement, though, since GCMs cannot adequately capture important features such as the Madden–Julian oscillation and convectively-coupled waves [31,39]. Various convective parameterizations have been developed over the past half century, and they vary in effectiveness [8,40]. Some of the most popular convective parameterizations utilized in contemporary GCMs are quasi-equilibrium models [9].

Quasi-equilibrium thinking was introduced by Arakawa and Schubert [1]. The premise is that regions of deep convection are in a quasi-equilibrium state where the convective available potential energy (CAPE) is nearly constant. Deep convection acts as an energy regulator – it holds the CAPE nearly constant by quickly consuming any excess of CAPE that develops. One popular convective parameterization based on quasi-equilibrium ideas was introduced by Betts and Miller [2]. A Betts–Miller scheme is used to parameterize convection for the model used here.

Since interactions between water vapor and large-scale dynamics are so important in tropical climate, and since GCMs parameterize this interaction, a fundamental question to ask about convective parameterizations is, What types of waves are supported by the parameterization? This question was addressed by, among others, Fuchs and Raymond [12] and Neelin and Yu [35], who studied the linear waves supported by Betts–Miller parameterizations. Frierson et al. [11] (hereafter FMP) recently addressed this question and found nonlinear precipitation front solutions for a simplified tropical climate model with a Betts–Miller convective parameterization. Their model has the form of shallow water equations and a water vapor equation coupled by a nonlinear precipitation term. It is intermediate in complexity between simple models and full GCMs, and it is similar in form to the Quasi-Equilibrium Tropical Circulation Model of Neelin and Zeng [36].

As was just explained, the simplified tropical climate model of FMP is used as a framework for studying the waves supported by convective parameterizations; in addition, the model has a second purpose: to provide a new mathematical theory for the propagation and interaction of *precipitation fronts*. By a precipitation front, we mean the boundary between a convective, precipitating region and a nonconvective, nonprecipitating region. Areas of transition between precipitating and nonprecipitating regions over scales of roughly 1,500 km have been seen in observational studies [32,41–43]. For instance, the Madden–Julian oscillation and convectively-coupled waves are examples of propagating convective regions with spatial scales of thousands of kilometers. Convectively-coupled waves are seen in observations of outgoing longwave radiation, which is a proxy for cloudiness – hence the name *convectively-coupled waves*. There has been a large amount of theoretical work to explain the spatial structures and slow phase speeds of the convectively-coupled Kelvin wave ($\approx$15 m/s) and the Madden–Julian oscillatioon ($\approx$5 m/s) [7,28–30,33,34,45,46], but no theory is yet generally accepted for these waves.

In this paper, exact analytical precipitation front solutions are found to the simplified tropical climate model of FMP. Whereas FMP found discontinuous precipitation front solutions, we show that precipitation fronts are realizable with continuous spatial structure; this clarifies the numerical results of FMP, which showed continuous precipitation fronts. These precipitation fronts are solutions when no forcing or dissipation besides convective heating is included in the model. For all choices of model parameter values that are typically used, we show that there are precipitation front solutions, and the structure of the fronts depends on the model parameter values. More work with the model used here is presented by Pauluis et al. [37], who discuss the nonlinear interaction between precipitation and coupled convective-gravity waves, and Khouider and Majda [21,22], who add realistic geophysical effects to the model used here. A high-resolution balanced numerical scheme for this model with rotational effects was also recently developed by Khouider and Majda [19,20].

1.2 Outline

The model of FMP will be presented in Sect. 2, and their precipitation front solutions will be reviewed in Sect. 3. Precipitation fronts are solutions where the spatial domain is divided into two regions, and the precipitation (and other model variables) changes abruptly at the boundary of the two regions. In one region the water vapor is below saturation and there is no precipitation, and in the other region the water vapor is above saturation level and there is precipitation. The boundary between the two regions is a free boundary that moves at a constant speed. It was shown that the allowed boundary speeds classify the fronts into three types: drying fronts, slow moistening fronts, and fast moistening fronts. The adjectives "drying" and "moistening" refer to whether the boundary is moving toward the saturated region or the unsaturated region. The slow and fast moistening fronts, however, violate Lax's stability criterion for moving discontinuities in hyperbolic systems (the precipitation is discontinuous at the boundary) [23,26]. Nevertheless, FMP demonstrated that all three types of fronts are robustly realizable numerically. In this paper the realizability of all three types of fronts is demonstrated further, including the detailed structure with finite relaxation times, both analytically and numerically.

The results in this paper generalize those of FMP in the following way. To arrive at their results, FMP took a model parameter to its limiting value. In their model, the convective adjustment time τ_c is the time scale over which the atmosphere adjusts to convection. For the Betts–Miller parameterization scheme, the moisture and temperature are relaxed back to reference profiles, and τ_c is the relaxation time. FMP took the limit of instantaneous convective adjustment, $\tau_c \to 0$. Here finite adjustment times ($\tau_c \neq 0$) are considered, and the results of FMP are obtained in the limit $\tau_c \to 0$. The *exact analytical structure* of the precipitation fronts for $\tau_c \neq 0$ is developed in Sect. 4. From the viewpoint of applied mathematics, the nonlinear relaxation system that is studied has novel phenomena as well as features in common with established applied mathematical theories of relaxation limits for conservation laws [5,16,18] and waves in reacting gas flows [6,3,25].

In Sect. 5 the spatial structure of the fronts is illustrated. Finally, in Sect. 6, the slope of the precipitation fronts is investigated in order to assess the practical physical dimensions of the fronts with finite relaxation times. As mentioned earlier, the precipitation is discontinuous for $\tau_c \to 0$. Although the precipitation is continuous for $\tau_c \neq 0$, it can have a very steep gradient for small τ_c and certain other situations. These other situations arise because the slope of the front depends on four parameters: the adjustment time τ_c, the front velocity, and two other parameters that will be introduced below.

2 A simplified tropical climate model

2.1 Derivation of the simplified tropical climate model

The simplified tropical climate model used here is a barotropic–first baroclinic mode model with a vertically averaged moisture. The equations for the barotropic and first baroclinic modes are derived from a Galerkin projection of the hydrostatic Boussinesq equations, which are

$$\frac{\partial \mathbf{U}}{\partial t} + \mathbf{U}\cdot\nabla\mathbf{U} + W\frac{\partial \mathbf{U}}{\partial z} + \beta y\mathbf{U}^{\perp} = -\nabla\Phi + S_{\mathbf{U}}, \tag{1}$$

$$\nabla\cdot\mathbf{U} + \frac{\partial W}{\partial z} = 0, \tag{2}$$

$$\frac{\partial \Theta}{\partial t} + \mathbf{U}\cdot\nabla\Theta + W\frac{\partial \Theta}{\partial z} + \frac{N^2\theta_0}{g}W = S_{\Theta}, \tag{3}$$

$$\frac{\partial \Phi}{\partial z} = g\frac{\Theta}{\theta_0}, \tag{4}$$

$$W\big|_{z=0,H} = 0, \tag{5}$$

where the last equation represents rigid lid boundary conditions at the surface $z = 0$ and the top of the troposphere $z = H$. The coordinates x, y, and z are the zonal, meridional, and vertical coordinates. $\mathbf{U} = (U, V)$ is the horizontal (zonal and meridional) velocity, W is the vertical velocity, Φ is the pressure, and Θ is the potential temperature anomaly. The full potential temperature of the system (including the background state) is actually

$$\Theta_{\text{total}} = \theta_0 + \frac{d\bar{\Theta}}{dz}z + \Theta.$$

Table 1 Model parameters and scales

Parameter	Derivation	Value	Description
c	NH/π	50 m/s	Velocity scale
β		$2.28 \times 10^{-11}\,\mathrm{m}^{-1}\,\mathrm{s}^{-1}$	Variation of Coriolis parameter
L	$\sqrt{c/\beta}$	1,500 km	Equatorial length scale
T	$\frac{L}{c}$	8.3 h	Equatorial time scale
θ_0		300 K	Typical atmospheric temperature
g		$9.8\,\mathrm{m/s}^2$	Gravitational acceleration
c_p		1,000 J/K/kg	Specific heat at constant pressure
N		$10^{-2}\,\mathrm{s}^{-1}$	Buoyancy frequency
H		16 km	Tropopause height
$\bar{\alpha}$	$\frac{HN^2\theta_0}{\pi g}$	15 K	Potential temperature scale
W_0	$\frac{H}{\pi T}$	0.18 m/s	Vertical velocity scale
L_v		2.5×10^6 J/kg	Latent heat of vaporization
$c_p\bar{\alpha}/L_\mathrm{v}$		6×10^{-3}	Scale factor for scaled moisture
α			Parameter in moisture saturation profile $\tilde{q}(\theta)$
$\bar{Q}$			Background mean moisture gradient (or gross moisture stratification)
c_d	c	50 m/s	Dry gravity wave speed
c_m	$\sqrt{\frac{1-\bar{Q}}{1+\alpha}}$		Moist gravity wave speed
τ_c			Convective adjustment time (or moisture relaxation time)
s			Front velocity
a	$-\frac{1+\alpha}{s}\frac{c_\mathrm{m}^2-s^2}{1-s^2}$		$a(s) > 0$ if and only if s is an allowed front speed
L_c	τ_c/a		Convective length scale

The background potential temperature appears in the model in the buoyancy frequency N^2, which is defined as

$$N^2 = \frac{g}{\theta_0}\frac{\mathrm{d}\bar{\Theta}}{\mathrm{d}z}.$$

The symbol $\mathbf{U}^\perp$ represents the orthogonal vector with components $(-V, U)$. $S_\mathbf{U}$ and S_Θ are source terms for the momentum and temperature. The material derivative is

$$\begin{aligned}\frac{D}{Dt} + W\frac{\partial}{\partial z} &= \frac{\partial}{\partial t} + \mathbf{U}\cdot\nabla + W\frac{\partial}{\partial z}\\ &= \frac{\partial}{\partial t} + U\frac{\partial}{\partial x} + V\frac{\partial}{\partial y} + W\frac{\partial}{\partial z},\end{aligned}$$

where ∇ is the horizontal gradient. The parameters used in this paper are listed in Table 1.

The barotropic–first baroclinic mode equations are derived from the hydrostatic Boussinesq equations by using a vertical Galerkin projection. The inner product used for the projection is

$$\langle F, G\rangle = \frac{1}{H}\int_0^H F(z)G(z)\,\mathrm{d}z.$$

Due to the boundary condition (5), the vertical velocity W is expanded in terms of the basis $\{\sqrt{2}\sin(k\pi z/H)\}_{k=1}^\infty$. For consistency in the hydrostatic Boussinesq equations (1)–(5), and also to represent prominent features of deep convection in the tropical atmosphere, the potential temperature Θ is also expanded in terms of this sine basis, whereas the horizontal velocity $\mathbf{U}$ and the pressure Φ are then expanded in terms of the basis $\{\sqrt{2}\cos(k\pi z/H)\}_{k=0}^\infty$. With the barotropic–first baroclinic mode approximation, only the barotropic mode ($k = 0$) and the first baroclinic mode ($k = 1$) are kept; that is, we impose the ansatz

$$\begin{pmatrix}\mathbf{U}\\ \Phi\end{pmatrix}(x, y, z, t) = \begin{pmatrix}\bar{\mathbf{u}}\\ \bar{p}\end{pmatrix}(x, y, t) + \begin{pmatrix}\mathbf{u}\\ p\end{pmatrix}(x, y, t)\sqrt{2}\cos\left(\frac{\pi z}{H}\right), \tag{6}$$

$$\begin{pmatrix} W \\ \Theta \\ S_\Theta \end{pmatrix}(x, y, z, t) = \begin{pmatrix} w \\ \theta \\ P \end{pmatrix}(x, y, t)\sqrt{2}\sin\left(\frac{\pi z}{H}\right), \tag{7}$$

where the only source S_Θ will be the precipitation P, and we set $S_{\mathbf{U}} = 0$. The hydrostatic equation (4) then gives the relation

$$p = -\frac{H}{\pi}\frac{g}{\theta_0}\theta,$$

and the continuity equation (2) yields

$$w = -\frac{H}{\pi}\nabla \cdot \mathbf{u}. \tag{8}$$

The variables are converted to nondimensional form using the dry gravity wave speed $c = NH/\pi \approx 50\,\text{m/s}$, the equatorial deformation length $L = \sqrt{c/\beta} \approx 1500\,\text{km}$, the time scale $T = L/c \approx 8\,\text{h}$, the temperature scale $\bar{\alpha} = HN^2\theta_0/\pi g \approx 15\,\text{K}$, and the pressure scale c^2. Table 1 lists the scales used and their definitions. Using the Galerkin projection outlined above, the barotropic–first baroclinic mode equations are, with nondimensional variables now,

$$\frac{\partial \bar{\mathbf{u}}}{\partial t} + \bar{\mathbf{u}} \cdot \nabla \bar{\mathbf{u}} + \mathbf{u} \cdot \nabla \mathbf{u} + (\nabla \cdot \mathbf{u})\mathbf{u} + y\bar{\mathbf{u}}^\perp = -\nabla \bar{p}, \tag{9}$$

$$\nabla \cdot \bar{\mathbf{u}} = 0, \tag{10}$$

$$\frac{\partial \mathbf{u}}{\partial t} + \bar{\mathbf{u}} \cdot \nabla \mathbf{u} + \mathbf{u} \cdot \nabla \bar{\mathbf{u}} + y\mathbf{u}^\perp = \nabla \theta, \tag{11}$$

$$\frac{\partial \theta}{\partial t} + \bar{\mathbf{u}} \cdot \nabla \theta - \nabla \cdot \mathbf{u} = P. \tag{12}$$

where P is the nondimensional precipitation. The parameterization for the precipitation will be given later. The other source terms have been dropped and will not be considered here. FMP gives more details of this derivation.

In the simplified tropical climate model derived by FMP, the moisture equation that accompanies the barotropic–first baroclinic mode equations is

$$\frac{\partial q}{\partial t} + \bar{\mathbf{u}} \cdot \nabla q + \bar{Q}\nabla \cdot \mathbf{u} = -P, \tag{13}$$

where q is the vertically averaged mixing ratio for water vapor, scaled by the nondimensional quantity $c_p\bar{\alpha}/L_\text{v}$. ($c_p$ is the specific heat at constant pressure, $\bar{\alpha}$ is the temperature scale, and L_v is the latent heat of vaporization.) We omit the overbar on the vertically averaged mixing ratio since it is the only moisture of the dynamical model. P is the same nondimensional precipitation that appears in (12). The constant, nondimensional parameter $\bar{Q}$, which is sometimes called the *gross moisture stratification*, arises from a background mixing ratio. See FMP for a detailed derivation of this equation. The variable q will be referred to simply as the *moisture* throughout this paper. The barotropic–first baroclinic mode equations (9)–(12) and the moisture equation (13) make up the simplified tropical climate model. Further simplifications will be made later.

The model described above has a vertical structure with only one baroclinic mode. One might suspect that a model with such a crude vertical structure would not be able to capture many features of the observed atmosphere. While such models can capture some features of the large-scale circulation [36,11], there are many details that are not represented. A model with two baroclinic modes of vertical structure can capture more details [21,22], and a model with full vertical structure can presumably represent the atmosphere in full, but such models would add more levels of complexity. For the purposes of this paper, the setting of one baroclinic mode is chosen for its simplicity so that some analytical results can be found.

2.2 Precipitation parameterization

On the large scales (∼1,500 km) considered here, the formulation of Betts and Miller [2] is a natural choice for modelling precipitation. In this model, when the moisture exceeds a reference saturation profile, it is relaxed back to saturation over a time scale of a few hours. Mathematically, this takes the form

$$P = \frac{1}{\tau_c}(q - \tilde{q}(\theta))^+, \tag{14}$$

where τ_c is the relaxation time, $\tilde{q}(\theta)$ is the prescribed reference profile for moisture saturation, and the superscript $^+$ denotes the positive part:

$$(q - \tilde{q})^+ = \begin{cases} q - \tilde{q} & \text{if } q - \tilde{q} > 0, \\ 0 & \text{if } q - \tilde{q} \leq 0. \end{cases}$$

Neelin and Zeng [36] and Betts and Miller [2] use relaxation times of order $\tau_c \approx 2\,\text{h}$, whereas Bretherton et al. [4] estimate $\tau_c \approx 12\,\text{h}$ from current observations.

Two common choices are made for the saturation moisture profile. The simplest choice mathematically is a constant moisture threshold,

$$\tilde{q}(\theta) = \hat{q}.$$

This is justified physically since atmospheric temperatures in the tropics are approximately uniform. The other common choice, used by Neelin and Zeng [36], is a linear profile,

$$\tilde{q}(\theta) = \theta. \tag{15}$$

This is known as the CAPE parameterization. The CAPE (convectively available potential energy) for the model used here is $q - \theta$. Thus, for this choice of $\tilde{q}(\theta)$, CAPE is kept in quasi-equilibrium. Convection schemes such as those of Arakawa and Schubert [1] and Betts and Miller [2], which are used in full GCMs, would reduce to this in the first baroclinic mode system. The parameterization used here is therefore a simplified model for the behavior of a GCM. See Smith [40] for more information on convective parameterization schemes. A combination of these two choices, utilized by FMP, will be used here:

$$\tilde{q}(\theta) = \hat{q} + \alpha\theta.$$

In FMP it was established that the convective parameter α must satisfy $-\bar{Q} < \alpha$ for uniform stability, and $\hat{q}$ should be nonnegative. Regions of space where $P = 0$ will be referred to as *unsaturated* or *dry* regions interchangeably, and regions of space where $P > 0$ will be referred to as *saturated* or *moist* regions interchangeably.

2.3 Conservation principles

Several conservation principles exist for this simplified tropical climate model. First, the equivalent potential temperature $\theta_e = q + \theta$ is conserved:

$$\frac{\bar{D}\theta_e}{Dt} = (1 - \bar{Q})\nabla \cdot \mathbf{u},$$

where advection by the barotropic velocity is denoted by

$$\frac{\bar{D}}{Dt} = \frac{\partial}{\partial t} + \bar{\mathbf{u}} \cdot \nabla.$$

This quantity θ_e is also sometimes called the *moist static energy*, since it is the sum of thermal energy and latent energy stored as moisture that could be released by condensation.

Second, the variable $Z = q + \bar{Q}\theta$ is decreasing along barotropic particle paths:

$$\frac{\bar{D}Z}{Dt} = -(1 - \bar{Q})P \leq 0.$$

The inequality holds because, as will be shown below, $\bar{Q}$ must satisfy $\bar{Q} < 1$ and the precipitation is nonnegative by definition (14).

Finally, the system conserves a total energy, which is the sum of a dry energy and a moist energy. The dry energy density is the sum of kinetic and available potential energy terms, and it is given by

$$\varepsilon_{\mathrm{d}} = \frac{1}{2}(|\bar{\mathbf{u}}|^2 + |\mathbf{u}|^2 + \theta^2).$$

The moist energy density is related to Z, and it is given by

$$\varepsilon_{\mathrm{m}} = \frac{1}{2}\frac{(q + \bar{Q}\theta)^2}{(1 - \bar{Q})(\alpha + \bar{Q})}. \tag{16}$$

The energy must be positive definite so that it can be used as a norm; therefore, from (16) it follows that $1 - \bar{Q}$ and $\alpha + \bar{Q}$ must have the same sign. From (9)–(13) the total energy density $\varepsilon = \varepsilon_d + \varepsilon_m$ then satisfies

$$\int \varepsilon(t)\,\mathrm{d}x\,\mathrm{d}y = \int \varepsilon(0)\,\mathrm{d}x\,\mathrm{d}y - \int_0^t \int \frac{q - \alpha\theta}{\alpha + \bar{Q}} P\,\mathrm{d}x\,\mathrm{d}y\,\mathrm{d}t. \tag{17}$$

When moisture is ignored, the total dry energy is conserved; the addition of moisture is expected to dissipate energy through precipitation. In order for (17) to represent dissipation of energy, the last term must satisfy

$$\frac{q - \alpha\theta}{\alpha + \bar{Q}} P \geq 0.$$

Since $P \geq 0$ by definition (14), and since $q - \alpha\theta$ is also positive when $P \neq 0$ (again by (14)), this occurs when α and $\bar{Q}$ satisfy

$$-\bar{Q} < \alpha < +\infty. \tag{18}$$

Another constraint on $\bar{Q}$ is obtained by recalling that $1 - \bar{Q}$ and $\alpha + \bar{Q}$ must have the same sign to ensure the moist energy density (16) is positive:

$$\bar{Q} < 1. \tag{19}$$

These constraints on α, $\bar{Q}$ will be used throughout the paper. Note that this energy conservation principle is *independent of relaxation time* τ_{c}.

2.4 Gradient equations

It was shown by FMP that, in the absence of a barotropic wind, the variables $\mathbf{u}$, θ, q satisfy a smoothness property, which we summarize now. This is shown by producing an energy estimate for the gradient of the simplified tropical climate model (9), (10), (11), (12) and (13). The assumption $\bar{\mathbf{u}} = 0$ here is crucial, since the barotropic–baroclinic interaction term makes the estimate invalid otherwise. Another key feature of the estimate is that it is *independent of relaxation time* τ_{c}.

Setting the barotropic velocity to zero in (9), (10), (11), (12) and (13) and then taking the gradient gives the gradient equations:

$$\frac{\partial \nabla u}{\partial t} = y\nabla v + v\hat{\mathbf{y}} + \frac{\partial \nabla \theta}{\partial x}, \tag{20}$$

$$\frac{\partial \nabla v}{\partial t} = -y\nabla u - u\hat{\mathbf{y}} + \frac{\partial \nabla \theta}{\partial y}, \tag{21}$$

$$\frac{\partial \nabla \theta}{\partial t} = \nabla(\nabla \cdot \mathbf{u}) + \nabla P, \tag{22}$$

$$\frac{\partial \nabla q}{\partial t} = -\bar{Q}\nabla(\nabla \cdot \mathbf{u}) - \nabla P. \tag{23}$$

We define the gradient energy density to be

$$\varepsilon_{\text{grad}} = \frac{1}{2}\left(|\nabla \mathbf{u}|^2 + |\nabla\theta|^2 + \frac{(\nabla q + \bar{Q}\nabla\theta)^2}{(1-\bar{Q})(\alpha+\bar{Q})}\right).$$

Under the evolution of (20)–(23), the gradient energy satisfies

$$\begin{aligned}\int \varepsilon_{\text{grad}}(t)dxdy &= \int \varepsilon_{\text{grad}}(0)\mathrm{d}x\mathrm{d}y + \int_0^t \int \left(v\frac{\partial u}{\partial y} - u\frac{\partial v}{\partial y}\right)\mathrm{d}x\mathrm{d}y\mathrm{d}t \\ &\quad - \int_0^t \int \frac{|\nabla(q-\alpha\theta)|^2}{\alpha+\bar{Q}} P'\mathrm{d}x\mathrm{d}y\mathrm{d}t \\ &\leq \int \varepsilon_{\text{grad}}(0)\mathrm{d}x\mathrm{d}y + \int_0^t \int \left(v\frac{\partial u}{\partial y} - u\frac{\partial v}{\partial y}\right)\mathrm{d}x\mathrm{d}y\mathrm{d}t,\end{aligned}$$

where P' is the derivative of P with respect to moisture deficit $q-\tilde{q}$. Since $P' \geq 0$, the third term above is sign definite and can be dropped to get the inequality. This inequality shows that, for any finite time interval, $\nabla\mathbf{u}$, $\nabla\theta$, ∇q are bounded in L^2 if bounded initially. Therefore, by Sobolev's Lemma [10], smooth initial conditions cannot develop discontinuities in $\mathbf{u}$, θ, q in a single space dimension. In particular, for one-dimensional fronts, u, θ, q are continuous if continuous initially.

Since this result is *independent of relaxation time* τ_c, it still holds in the limit $\tau_c \to 0$. However, since there are no energy estimates for second derivatives (because the terms with P'' are no longer sign definite), one can expect discontinuities in $\nabla\mathbf{u}$, $\nabla\theta$, ∇q to develop in the limit $\tau_c \to 0$. Formal solutions of this type were demonstrated by FMP, and they will be summarized in the next section. Then fronts with *continuous* $\nabla\mathbf{u}$, $\nabla\theta$, ∇q, for $\tau_c \neq 0$ will be developed in the remainder of the paper.

3 Precipitation fronts for instantaneous convective adjustment ($\tau_c \to 0$)

3.1 Instantaneous convective adjustment

In the formal limit $\tau_c \to 0$, convective adjustment takes place instantaneously. This is known as "strict quasi-equilibrium." (Recall that the parameterization choice (15) kept CAPE in a state of quasi-equilibrium for $\tau_c \neq 0$.) Since the gradient estimates mentioned above are independent of τ_c, the equations arising from the limit $\tau_c \to 0$ will be well-posed formally.

The free boundary problem in the limit $\tau_c \to 0$ was studied by FMP. The boundary is between an unsaturated region with no precipitation and a saturated region with precipitation. Before getting into the free boundary problem, disturbances that remain within one region are first described here. The linear waves for the model behave differently for the saturated and unsaturated regions; specifically, moist disturbances have a slower wave speed than dry disturbances, as has been reported in observational studies such as that of Wheeler and Kiladis [42]. To see this for our model, note that dry disturbances ($P = 0$), in the absence of a barotropic wind, satisfy

$$\begin{aligned}\frac{\partial \mathbf{u}}{\partial t} + y\mathbf{u} - \nabla\theta &= 0, \\ \frac{\partial \theta}{\partial t} - \nabla\cdot\mathbf{u} &= 0.\end{aligned}$$

These are the well-known linearized shallow water equations on a beta-plane (see [13] or [27]). The Kelvin wave of this system has speed $c_d = 1$ in our nondimensional units. On the other hand, for a moist disturbance in the limit $\tau_c \to 0$, the moisture is saturated at its reference value,

$$q = \hat{q} + \alpha\theta.$$

Using this relation, and adding Eq. (12) and (13) to cancel P, one obtains

$$\frac{\partial \mathbf{u}}{\partial t} + y\mathbf{u} - \nabla\theta = 0,$$
$$\frac{\partial \theta}{\partial t} - \frac{1-\bar{Q}}{1+\alpha}\nabla\cdot\mathbf{u} = 0.$$

The Kelvin wave of this system has speed

$$c_{\mathrm{m}} = \sqrt{\frac{1-\bar{Q}}{1+\alpha}}. \tag{24}$$

Since $-\bar{Q} < \alpha$, the moist wave speed c_{m} is slower than the dry wave speed $c_{\mathrm{d}} = 1$. The parameters $\bar{Q}, \alpha$ will be chosen so that $c_{\mathrm{m}} \approx 15$ m/s ($c_{\mathrm{m}} \approx 0.3 c_{\mathrm{d}}$), in agreement with observational data such as that of Wheeler and Kiladis [42].

These dry and moist Kelvin waves are solutions propagating entirely within either the dry or moist region. More interesting waves arise from the free boundary problem, where the boundary between the dry and moist regions propagates. These solutions are called *precipitation fronts* and were studied by FMP for the limit $\tau_{\mathrm{c}} \to 0$. These solutions will be reviewed next, and then the main result of this paper—the exact analytical structure of precipitation fronts for $\tau_{\mathrm{c}} \neq 0$—will be presented.

3.2 One-dimensional setup

In the limit $\tau_{\mathrm{c}} \to 0$, FMP found discontinuous precipitation fronts for the simplified tropical climate model presented above. The equations used were the one-dimensional equations

$$\frac{\partial u}{\partial t} = \frac{\partial \theta}{\partial x}, \tag{25}$$
$$\frac{\partial \theta}{\partial t} = \frac{\partial u}{\partial x} + P, \tag{26}$$
$$\frac{\partial q}{\partial t} = -\bar{Q}\frac{\partial u}{\partial x} - P, \tag{27}$$

where the precipitation P was defined in (14) as

$$P = \frac{1}{\tau_{\mathrm{c}}}(q - \tilde{q}(\theta))^{+}.$$

Here the barotropic wind was set to zero, and the Coriolis force was ignored. Since the Coriolis force vanishes at the equator, this setup can be considered zonal circulation at the equator. These one-dimensional zonal equations are meaningful in the tropics since many important features of tropical dynamics – such as the Walker circulation, propagation of superclusters, and the Madden–Julian oscillation – occur in the zonal direction.

Although the model variables u, θ, q are guaranteed to remain continuous if they were initially (as was mentioned earlier), the derivatives of these quantities might be discontinuous. Taking the x-derivative of (25)–(27) gives

$$\frac{\partial w}{\partial t} = -\frac{\partial \theta_x}{\partial x}, \tag{28}$$
$$\frac{\partial \theta_x}{\partial t} = -\frac{\partial w}{\partial x} + \frac{\partial P}{\partial x}, \tag{29}$$
$$\frac{\partial q_x}{\partial t} = \bar{Q}\frac{\partial w}{\partial x} - \frac{\partial P}{\partial x}, \tag{30}$$

where $w = -u_x$ from (8). Now suppose there is a discontinuity in w, θ_x, and q_x propagating at speed s. The jump conditions for (28)–(30) at the discontinuity are

$$-s[w] = -[\theta_x], \tag{31}$$
$$-s[\theta_x] = -[w] + [P], \tag{32}$$
$$-s[q_x] = \bar{Q}[w] - [P], \tag{33}$$

where $[w] = w_+ - w_-$ is the jump in w across the discontinuity.

Before considering the precipitation fronts, notice that there are solutions to the jump conditions that occur entirely within the dry or moist region. For a discontinuity within the dry region, where $P = 0$, Eq. (31) and (32) yield $s = \pm 1 = \pm c_{\mathrm{d}}$, the dry wave speed. This is a dry gravity wave, the analog (without rotation) of the Kelvin wave solution discussed earlier. On the other hand, for a discontinuity entirely within the moist region, (32) and (33) can be added to give

$$-s[\theta_x] - s[q_x] = -(1 - \bar{Q})[w]. \tag{34}$$

In the limit $\tau_{\mathrm{c}} \to 0$, the moisture in the moist region is $q = \hat{q} + \alpha\theta$, so that (34) and (31) yield $s = \pm\sqrt{1 - \bar{Q}/1 + \alpha} = \pm c_{\mathrm{m}}$, the moist wave speed. This is a moist gravity wave, the analog of the moist Kelvin wave solution discussed earlier. These solutions were to be expected, since the disturbance speed within the moist or dry region is the same whether the disturbance is continuous or not.

3.3 Three branches of precipitation fronts

Now consider a discontinuity at the *interface between a dry and a moist region*. Without loss of generality, assume the dry region is initially on the negative side of the real axis, and the moist region is on the positive side of the real axis. Then $s < 0$ corresponds to a moistening front, and $s > 0$ corresponds to a drying front. It is shown by FMP that the front speed s must satisfy one of

$$c_{\mathrm{m}} < s < c_{\mathrm{d}} \quad \text{Drying Front,} \tag{35}$$

$$-c_{\mathrm{m}} < s < 0 \quad \text{Slow Moistening Front,} \tag{36}$$

$$s < -c_{\mathrm{d}} \quad \text{Fast Moistening Front.} \tag{37}$$

The drying front has speed between the moist and dry wave speeds, which is precisely the range of speeds needed for stability of the front under Lax's stability criterion. The moistening fronts, on the other hand, violate Lax's stability criterion; moreover, the fast moistening fronts travel at speeds that, physically, are unreasonably fast. Nonetheless, it was shown by FMP that the moistening fronts are realizable as numerical solutions to (25), (26) and (27) for nonzero τ_{c}. In the rest of this paper, the following questions are addressed: What is the analytical structure of these fronts for nonzero τ_{c}? How is the structure influenced by the model parameters?

4 Precipitation fronts for nonzero convective adjustment time ($\tau_{\mathrm{c}} \neq 0$)

In this section the structure of the precipitation fronts for $\tau_{\mathrm{c}} \neq 0$ will be derived. The variables u, θ, q will have a simple linear structure in the dry region, as they did for the case $\tau_{\mathrm{c}} = 0$ in the previous section. In the moist region, the front will be approximately linear; it will also include a correction term for $\tau_{\mathrm{c}} \neq 0$.

To find the moist region solution, the gradient equations (28)–(30) will be solved first, and their solutions will be integrated to get solutions to (25), (26) and (27). The solution to (28), (29), (30) is derived by seeking travelling wave solutions that are functions of $x - st/\tau_{\mathrm{c}}$. A simple ordinary differential equation (ODE) with exponential solutions will arise, and the three branches of precipitation fronts will arise by excluding solutions that grow exponentially in favor of those that tend to a finite limit.

In short, to calculate the precipitation fronts, use constant dry region solutions w, θ_x, q_x to (28), (29) and (30), find moist region travelling wave solutions w, θ_x, q_x to (28), (29), (30) as functions of $x - st/\tau_{\mathrm{c}}$, match the dry and moist region solutions at the boundary of the two regions, and integrate w, θ_x, q_x to find solutions u, θ, q to (25), (26) and (27). This is the task of this section. Many of the actual calculations are relegated to appendices.

4.1 Dry region solution to derivative equations

The gradient equations (28), (29) and (30) have constant solutions for the dry region ($P = 0$) of the form

$$w = w_-, \tag{38}$$

$$\theta_x = \theta_{x-}, \tag{39}$$

$$q_x = q_{x-} \tag{40}$$

provided the *dry region constraint*

$$q_{x-} > \alpha\theta_{x-} \tag{41}$$

is met to ensure the moisture is unsaturated ($q < \tilde{q}$) and the precipitation is zero.

The next step is to find solutions for the moist region, and then the dry and moist solutions must be matched at their boundary.

4.2 Moist region solution to derivative equations

To have a moist region solution, the *moist region constraint*

$$q - \alpha\theta - \hat{q} > 0 \tag{42}$$

must be met. We define new variables to rewrite Eqs. (28), (29) and (30) in a simpler form. The new variables are useful for waves in moist regions, and they are

$$\theta_e = \theta + q, \quad Z = \bar{Q}\theta + q. \tag{43}$$

In terms of the variables w, $(\theta_e)_x$, Z_x, Eqs. (28), (29) and (30) are

$$\frac{\partial w}{\partial t} = \frac{1}{1-\bar{Q}}(Z_x - (\theta_e)_x)_x, \tag{44}$$

$$\frac{\partial (\theta_e)_x}{\partial t} = -(1-\bar{Q})w_x, \tag{45}$$

$$\frac{\partial Z_x}{\partial t} = -\frac{1}{\tau_c}((1+\alpha)Z_x - (\bar{Q}+\alpha)(\theta_e)_x), \tag{46}$$

where the moist region constraint (42) is assumed to be met. Note that the right hand sides of (44) and (45) are perfect x derivatives, which will allow us to easily integrate these two equations below. Also, (46) is a simple ODE that is coupled with (44) and (45) for the moment and will become an ODE for Z_x alone below.

For travelling wave solutions to the free boundary problem, let s be the constant speed of the boundary. Also, define the moving reference frame variable $\tilde{x} = x - st$, and, without loss of generality, assume the dry region is $\tilde{x} < 0$ and the moist region is $\tilde{x} > 0$. As a travelling wave ansatz, the moist region variables are written as functions of $\tilde{x}/\tau_c$:

$$w = w\left(\frac{x-st}{\tau_c}\right),$$

$$(\theta_e)_x = (\theta_e)_x\left(\frac{x-st}{\tau_c}\right),$$

$$Z_x = Z_x\left(\frac{x-st}{\tau_c}\right).$$

Inserting this ansatz into Eqs. (44), (45) and (46) gives

$$-s\frac{dw}{d(\tilde{x}/\tau_c)} = \frac{1}{1-\bar{Q}}\left(\frac{dZ_x}{d(\tilde{x}/\tau_c)} - \frac{d(\theta_e)_x}{d(\tilde{x}/\tau_c)}\right) \tag{47}$$

$$-s\frac{d(\theta_e)_x}{d(\tilde{x}/\tau_c)} = -(1-\bar{Q})\frac{dw}{d(\tilde{x}/\tau_c)} \tag{48}$$

$$-s\frac{dZ_x}{d(\tilde{x}/\tau_c)} = -((1+\alpha)Z_x - (\bar{Q}+\alpha)(\theta_e)_x) \tag{49}$$

where the *moist region constraint*

$$\int_0^{\tilde{x}} q_{\tilde{x}} - \alpha\theta_{\tilde{x}}\, d\tilde{x} > 0 \tag{50}$$

must be satisfied. This version (50) of the moist region constraint is equivalent to (42) above, since $\hat{q} = q(0) - \alpha\theta(0)$. It is sufficient to have

$$q_{\tilde{x}} - \alpha\theta_{\tilde{x}} > 0.$$

From (47) and (48), the variables w, $(\theta_e)_x$ can immediately be written in terms of Z_x as

$$w = \frac{1}{1-\bar{Q}} \frac{s}{1-s^2} Z_x + C_w \tag{51}$$

$$(\theta_e)_x = \frac{1}{1-s^2} Z_x + C_\theta, \tag{52}$$

where C_w and C_θ are constants of integration that will be determined later. Then the ODE (49) for Z_x becomes

$$\frac{dZ_x}{d(\tilde{x}/\tau_c)} = -aZ_x - b, \tag{53}$$

where

$$a = -\frac{1+\alpha}{s} \frac{c_m^2 - s^2}{1-s^2}, \tag{54}$$

$$b = \frac{\bar{Q}+\alpha}{s} C_\theta, \tag{55}$$

$$c_m = \sqrt{\frac{1-\bar{Q}}{1+\alpha}}. \tag{56}$$

c_m is the moist wave speed introduced in (24).

We take a respite from our calculation now to consider the coefficient of Z_x in (53). In order to rule out solutions that grow exponentially as $\tilde{x} \to +\infty$, we must have

$$a > 0.$$

As shown by (54) and (56), a depends on s, $\bar{Q}$, and α. For fixed $\bar{Q}$ and α satisfying (18) and (19), $a(s)$ is shown in Fig. 1. From this plot, or from examining the definition of a in (54), one finds $a(s) > 0$ for the *allowed front speeds*

$$c_m < s < 1, \tag{57}$$

$$-c_m < s < 0, \tag{58}$$

$$s < -1. \tag{59}$$

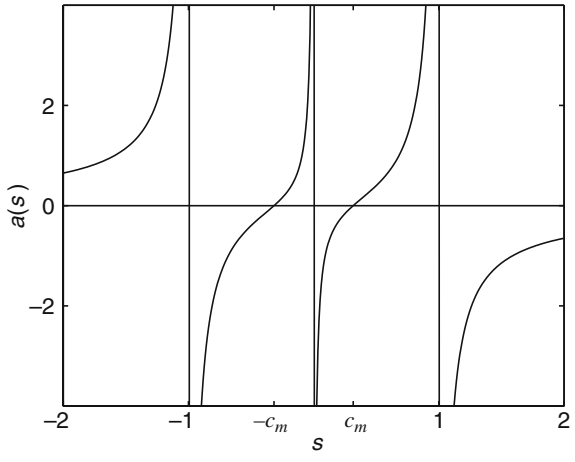

Fig. 1 A qualitative plot of $a(s)$ when $1 - \bar{Q} > 0$ and $\bar{Q} + \alpha > 0$. Values of s for which $a(s) > 0$ are allowed front speeds

These are precisely the three branches of allowed precipitation fronts found by FMP: drying fronts, slow moistening fronts, and fast moistening fronts. These three branches of fronts were summarized earlier here for $\tau_c \to 0$ in (35), (36) and (37).

Returning to the task of calculating w, θ_x, q_x, the next steps on the agenda are to integrate (53) to find Z_x, convert back to the variables w, θ_x, q_x, and match these moist regions solutions to the dry region solutions (38), (39) and (40) to get continuous solutions (as stated earlier, it is only in the limit $\tau_c \to 0$ that we expect w, θ_x, q_x to become discontinuous). These steps are carried out in Appendix A. The result is

$$w = w_+ - [w]\mathrm{e}^{-a\tilde{x}/\tau_c}, \tag{60}$$

$$\theta_x = \theta_{x+} - [\theta_x]\mathrm{e}^{-a\tilde{x}/\tau_c}, \tag{61}$$

$$q_x = q_{x+} - [q_x]\mathrm{e}^{-a\tilde{x}/\tau_c}, \tag{62}$$

where

$$w_+ := \lim_{\tilde{x}\to+\infty} w$$

is defined as the asymptotic moist region value of w, and

$$[w] = w_+ - w_-$$

is the jump in w across the boundary between the dry and moist regions. w_+ could equivalently be defined as

$$w_+ := \lim_{\tau_c\to 0} w.$$

θ_{x+} and q_{x+} are defined analogously. Expressions for w_+, θ_{x+}, q_{x+} in terms of other parameters are given in Appendix A. The important relations involving the new parameters are

$$s[w] = [\theta_x], \tag{63}$$

$$q_{x+} = \alpha\theta_{x+}, \tag{64}$$

$$[q_x] = \left(\frac{1-\bar{Q}}{s} - s\right)[w]. \tag{65}$$

(See Appendix A for more details.) These relations were also found by FMP for the limiting case $\tau_c \to 0$.

At this stage we can also calculate the precipitation. Using the forms of θ_x, q_x in (61) and (62), and using (64), we write

$$q_x - \alpha\theta_x = (q_{x-} - \alpha\theta_{x-})\mathrm{e}^{-a\tilde{x}/\tau_c}.$$

Note that this is positive because the dry region constraint (41) is $q_{x-} - \alpha\theta_{x-} > 0$. To have the precipitation be continuous at the boundary of the dry and moist regions, we must have $\hat{q} = q(0) - \alpha\theta(0)$. Therefore, the precipitation in the moist region is given by

$$\begin{aligned} P &= \frac{1}{\tau_c}(q - \alpha\theta - \hat{q})^+ = \frac{1}{\tau_c}\int_0^{\tilde{x}} (q_{\tilde{x}} - \alpha\theta_{\tilde{x}})\,\mathrm{d}\tilde{x} \\ &= \frac{1}{a}(q_{x-} - \alpha\theta_{x-})(1 - \mathrm{e}^{-a\tilde{x}/\tau_c}) \end{aligned} \tag{66}$$

Note that $P > 0$ for $a > 0$, the allowed front speeds. We also define P_+ as

$$P_+ = \lim_{\tilde{x}\to+\infty} P = \frac{1}{a}(q_{x-} - \alpha\theta_{x-}). \tag{67}$$

Using the definition of a from (54), and using (96) from Appendix A, P_+ can also be written as

$$P_+ = (1 - s^2)[w]. \tag{68}$$

And since there is no precipitation in the dry region, we have

$$P_- = 0.$$

The precipitation can then be written as

$$P = P_+(1 - \mathrm{e}^{-a\tilde{x}/\tau_\mathrm{c}}),$$

or, to put it in the same form as the moist region solutions (60)–(62),

$$P = P_+ - [P]\mathrm{e}^{-a\tilde{x}/\tau_\mathrm{c}}. \tag{69}$$

4.3 Integrating solutions to derivative equations

At this point solutions w, θ_x, q_x to the derivative Eqs. (28), (29) and (30) have been constructed, but the goal is to find solutions u, θ, q to the simplified tropical climate model (25), (26) and (27).

To find u, θ, q, integrate the solutions (38), (39) and (40) and (60), (61) and (62) for w, θ_x, q_x to obtain

$$u = -w_-\tilde{x} + f_u(t), \tag{70}$$
$$\theta = \theta_{x-}\tilde{x} + f_\theta(t), \tag{71}$$
$$q = q_{x-}\tilde{x} + f_q(t), \tag{72}$$

in the dry region and

$$u = -w_+\tilde{x} - \frac{\tau_\mathrm{c}}{a}[w]\mathrm{e}^{-a\tilde{x}/\tau_\mathrm{c}} + g_u(t), \tag{73}$$
$$\theta = \theta_{x+}\tilde{x} + \frac{\tau_\mathrm{c}}{a}[\theta_x]\mathrm{e}^{-a\tilde{x}/\tau_\mathrm{c}} + g_\theta(t), \tag{74}$$
$$q = q_{x+}\tilde{x} + \frac{\tau_\mathrm{c}}{a}[q_x]\mathrm{e}^{-a\tilde{x}/\tau_\mathrm{c}} + g_q(t) \tag{75}$$

in the moist region. The functions $f_u, f_\theta, f_q, g_u, g_\theta, g_q$ are determined by requiring u, θ, q to be continuous at $\tilde{x} = 0$ and by requiring (70), (71), (72) (73), (74) and (75) to actually be solutions to equations (25), (26) and (27). This work is carried out in Appendix B. The result is *the dry region solution*

$$u(\tilde{x}, t) = -w_-\tilde{x} + (\theta_{x-} - sw_-)t + u(0, 0), \tag{76}$$
$$\theta(\tilde{x}, t) = \theta_{x-}\tilde{x} + (s\theta_{x-} - w_-)t + \theta(0, 0), \tag{77}$$
$$q(\tilde{x}, t) = q_{x-}\tilde{x} + \alpha(s\theta_{x-} - w_-)t + \hat{q} + \alpha\theta(0, 0). \tag{78}$$

and the moist region solution

$$u(\tilde{x}, t) = -w_+\tilde{x} + \frac{\tau_\mathrm{c}}{a}[w](1 - \mathrm{e}^{-a\tilde{x}/\tau_\mathrm{c}}) + (\theta_{x-} - sw_-)t + u(0, 0) \tag{79}$$
$$\theta(\tilde{x}, t) = \theta_{x+}\tilde{x} - \frac{\tau_\mathrm{c}}{a}[\theta_x](1 - \mathrm{e}^{-a\tilde{x}/\tau_\mathrm{c}}) + (s\theta_{x-} - w_-)t + \theta(0, 0) \tag{80}$$
$$q(\tilde{x}, t) = q_{x+}\tilde{x} - \frac{\tau_\mathrm{c}}{a}[q_x](1 - \mathrm{e}^{-a\tilde{x}/\tau_\mathrm{c}}) + \alpha(s\theta_{x-} - w_-)t + \hat{q} + \alpha\theta(0, 0). \tag{81}$$

The similarity between the dry and moist region solutions is evident. In the limit $\tau_\mathrm{c} \to 0$, the moist region solutions will be of the same linear form as the dry region solutions. Although the solutions w, θ_x, q_x of (38), (39), (40), (60), (61) and (62) and the precipitation (69) were travelling waves, the solutions u, θ, q of (76), (77), (78), (80) and (81) are not precisely travelling waves, since they contain linear-in-time terms; this feature will be discussed below. Also note that the linear-in-time terms can be written in terms of θ_{x+} and w_+ by using

$$\theta_{x-} - sw_- = \theta_{x+} - sw_+, \tag{82}$$
$$s\theta_{x-} - w_- = s\theta_{x+} - c_\mathrm{m}^2 w_+, \tag{83}$$

which follow from (63), (68), and (85).

In the process of obtaining (76), (77), (78), (79), (80) and (81) (see Appendix B), three important constraints arise. The first two are

$$s = -\frac{\bar{Q} + \alpha}{q_{x-} - \alpha\theta_{x-}} w_-, \tag{84}$$

$$P_+ = \frac{\bar{Q} + \alpha}{1 + \alpha} w_+. \tag{85}$$

These are consistent with our physical intuition. The front speed has the same sign as the divergence in the dry region, so divergence in the dry region corresponds to a drying front, and convergence in the dry region corresponds to a moistening front. The formula for P_+ also makes physical sense, with precipitation proportional to the moist region convergence. The effect of α is to slightly increase the precipitation over the $\alpha = 0$ case given a value of w_+. And since we must have $P_+ > 0$, we have the new constraint

$$w_+ > 0, \tag{86}$$

so the moist region is a region of convergence.

4.4 Summary of the realizability of precipitation fronts

Here we summarize our demonstration of the realizability of the precipitation front solutions. In FMP precipitation front solutions were found using formal arguments for the limit of instantaneous convective adjustment ($\tau_c \to 0$). Three branches of precipitation fronts were found: drying fronts, slow moistening fronts, and fast moistening fronts. The two moistening fronts, which satisfy $s < -c_d$ and $-c_m < s < 0$, do not satisfy Lax's stability criterion [23,26], which requires the front speed to be intermediate between the disturbance speeds of the two adjacent regions: $c_m < s < c_d$. As was shown by Majda [26],
discontinuous fronts are linearly structurally stable if and only if Lax's stability criterion (and another condition) is satisfied.

Since the two moistening fronts violate Lax's stability criterion, it was not immediately clear that the moistening fronts would be stable, realizable solutions. FMP addressed this concern with numerical experiments for finite adjustment times ($\tau_c \neq 0$). Their results show how *discontinuous* initial conditions evolved into *continuous* precipitation front solutions for numerical simulations with *finite* adjustment times. This was the case for all three types of fronts, thereby demonstrating the robust realizability of all three fronts numerically (for $\tau_c \neq 0$) even though the moistening fronts violate Lax's stability criterion.

All three types of fronts were robustly realizable in FMP's numerical experiments, despite the stability theorem of [26], because the stability theorem holds only for *inviscid* conservation laws (or, in the case of this tropical climate model, the theorem holds only for relaxation systems in the limit of *instantaneous relaxation time*, $\tau_c \to 0$). When finite relaxation times are used, the theorem does not apply, and fronts that violate Lax's stability criterion might be realizable. The exact analytic solutions found in this paper show why all three types of fronts are realizable analytically for finite adjustment times. It is because, remarkably, there are exact, continuous precipitation front solutions to the model equations for finite relaxation times.

The three types of precipitation fronts (slow moistening, fast moistening, and drying) are reminiscent of the three types of wave fronts in reacting gas flow: flame fronts, weak detonations, and strong detonations [44]. Table 2 lays out the characteristics of the analogous fronts from the two theories. In the table, "subsonic" refers to a speed slower than the gravity wave speed, and "supersonic" refers to a speed faster than the gravity wave

Table 2 Analogy between precipitation fronts and reacting gas fronts

Precipitation front	Slow moistening front	Fast moistening front	Drying front
Reacting gas font	Flame front	Weak detonation	Strong detonation
Lax's shock inequalities	Violated	Violated	Satisfied
Front speed	Subsonic	Supersonic	Subsonic from one side, supersonic from the other
Realizability of precipitation front	Always	Always	Always
Realizability of reacting gas front	Unique speed arises as nonlinear eigenvalue problem	Only for special coefficient values of viscosity and heat reduction	Always

speed. For instance, since slow moistening fronts satisfy $|s| < c_{\mathrm{m}} < c_{\mathrm{d}}$, they are subsonic from the viewpoint of both the dry side and the moist side of the front; an analogous inequality is also true for flame fronts in reacting gas flows. Drying fronts and strong detonations are subsonic when viewed from one side of the front and supersonic when viewed from the other side. Interestingly, whereas all three types of precipitation fronts are always realizable, all three reacting gas fronts are not always realizable.

As indicated by Table 2, the three fronts from reacting gas flow satisfy front speed bounds analogous to those in (57), (58), and (59). Flame fronts, which are analogous to slow moistening fronts, propagate at speeds that are determined as a nonlinear eigenvalue problem through a subtle balance of reaction and diffusion [44]. Weak detonations, which are analogous to fast moistening fronts, are realizable only for special values of diffusion and reaction coefficients [6,25]. Strong detonations, which are analogous to drying fronts and satisfy Lax's shock inequalities as in (57), are always realizable [3,25]. The exact analytical solutions derived here show that all three types of precipitation fronts are realizable for finite relaxation times τ_{c}.

One significant difference between the system (25), (26) and (27) studied here and the system for reacting gas flow is that here the basic jump discontinuities occur in the derivative of the solution. Also, the nonlinear source term P involves the solution itself and not its derivative; this creates a smoother and more realizable background environment for the propagation of discontinuities in first derivatives. For reacting gas flow, on the other hand, both the discontinuities and nonlinear source terms occur at the level of primitive variables such as temperature.

The numerical simulations in Figs. 5 and 6 of [20] for the simplified tropical climate model provide further evidence for the robust realizability of all three types of precipitation fronts in general dynamical solutions with finite relaxation time including the fast moistening front. In particular, in Figs. 6 from [20], a fast moistening front arises from the interaction of the strong convergence zone of a dry gravity wave with a region of precipitation bounded by slow moistening and drying precipitation fronts. These results confirm the robust realizability of fast moistening fronts discussed in the present paper through traveling wave analysis in contrast with the rarely observed weak detonations of combustion theory.

5 Illustration of precipitation front structure

In this section, precipitation front solutions are constructed and illustrated to give a clearer picture of the analytical form in (76), (77), (78), (79), (80) and (81).

5.1 Constructing precipitation fronts

There are several parameters in the solutions (76), (77), (78), (79), (80) and (81), and several of these parameters are determined from others. In this subsection, we make clear which parameters must be chosen to construct precipitation front solutions.

Constructing precipitation fronts by specifying dry region solutions One can construct precipitation front solutions to, (25), (26) and (27) by specifying the dry region solutions:

1. Choose parameter values $\bar{Q}$ and α satisfying
$$\begin{aligned} \bar{Q} &< 1, \\ -\bar{Q} &< \alpha. \end{aligned}$$
2. Choose the constant dry region solution values θ_{x-} and q_{x-} satisfying
$$q_{x-} - \alpha\theta_{x-} > 0,$$
3. Choose the dry region convergence w_- satisfying one of
$$\begin{aligned} -\frac{q_{x-} - \alpha\theta_{x-}}{\bar{Q} + \alpha} < w_- < -\frac{q_{x-} - \alpha\theta_{x-}}{\bar{Q} + \alpha} c_{\mathrm{m}}, \\ 0 < w_- < \frac{q_{x-} - \alpha\theta_{x-}}{\bar{Q} + \alpha} c_{\mathrm{m}}, \\ \frac{q_{x-} - \alpha\theta_{x-}}{\bar{Q} + \alpha} < w_- \end{aligned}$$

corresponding, respectively, to the front speeds

$$\begin{aligned} c_{\mathrm{m}} &< s < 1, \\ -c_{\mathrm{m}} &< s < 0, \\ s &< -1. \end{aligned}$$

4. Choose $u(0,0)$ and $\theta(0,0)$, the values of u and θ at $x = t = 0$.

Step 3 above follows from (84) and (57), (58) and (59). Both the dry region solutions (76), (77) and (78) and the moist region solutions (79), (80) and (81) are then determined by these parameters. This is a seven-parameter ($\bar{Q}$, α, w_-, θ_{x-}, q_{x-}, $u(0,0)$, $\theta(0,0)$) family of solutions where four of the parameters are constrained and three parameters ($u(0,0)$, $\theta(0,0)$, and either θ_{x-} or q_{x-}) are free.

Constructing precipitation fronts using the convergence parameters w_- and w_+. Instead of specifying w_-, θ_{x-}, q_{x-} to construct precipitation front solutions, one could specify w_- and w_+. This can be seen once clearer relations among w_-, w_+, and the other parameters are established. From (84) and (96) one finds

$$w_- = \frac{c_{\mathrm{m}}^2 - s^2}{1 - s^2} w_+. \tag{87}$$

Note that, from (87), a can then be written as

$$a = -\frac{1+\alpha}{s} \frac{w_-}{w_+}. \tag{88}$$

Also, solving (87) for s gives

$$s = \pm \sqrt{\frac{c_{\mathrm{m}}^2 w_+ - w_-}{w_+ - w_-}}, \tag{89}$$

where the $\pm$ is determined by $s w_- < 0$ from (84). (Note that (88) and (89) show that a and s are functions of the ratio w_-/w_+.) Since $c_{\mathrm{m}} < 1$ and $w_+ > 0$, (89) shows that s will be an allowed front speed for the following values of w_- and w_+:

$$\begin{aligned} c_{\mathrm{m}} < s < 1 \quad &\text{for} \quad w_- < 0 < w_+, \\ -c_{\mathrm{m}} < s < 0 \quad &\text{for} \quad 0 < w_- < c_{\mathrm{m}}^2 w_+, \\ s < -1 \quad &\text{for} \quad 0 < w_+ < w_-. \end{aligned}$$

Note that the dry region constraint $q_{x-} - \alpha\theta_{x-} > 0$ (and therefore the moist region constraint as well) is automatically satisfied for allowed front speeds; to see this, note that (63) and (65) are used to determine q_{x-} and θ_{x-}, which then satisfy

$$q_{x-} - \alpha\theta_{x-} = -[w](1+\alpha)\frac{c_{\mathrm{m}}^2 - s^2}{s} = a P_+ > 0,$$

where $P_+ = (1 - s^2)[w]$ was used. The constant θ_{x+} or q_{x+} is then freely chosen, and the remaining parameters θ_{x-} and q_{x-} are determined using (63), (64) and (65).

Precipitation fronts can therefore be constructed in the following way:

1. Choose parameter values $\bar{Q}$ and α satisfying

$$\begin{aligned} \bar{Q} &< 1, \\ -\bar{Q} &< \alpha. \end{aligned}$$

2. Choose convergence values w_- and w_+ satisfying one of

$$\begin{aligned} w_- &< 0 < w_+, \\ 0 &< w_- < c_{\mathrm{m}}^2 w_+, \\ 0 &< w_+ < w_- \end{aligned}$$

corresponding, respectively, to the front speeds

$$\begin{aligned} c_{\mathrm{m}} &< s < 1, \\ -c_{\mathrm{m}} &< s < 0, \\ s &< -1. \end{aligned}$$

3. Choose either q_{x+} or θ_{x+} freely
4. Choose $u(0,0)$ and $\theta(0,0)$ freely.

Removing linear-in-time terms The precipitation front solutions (76), (77), (78), (79), (80) and (81) are not precisely travelling waves, since they include linear-in-time terms. The convergence w and the precipitation P, however, are always travelling waves, and the moisture q is a travelling wave for $\alpha = 0$. Furthermore, it is possible to remove some of the linear-in-time terms, since there is some freedom in choosing the parameters w_-, θ_{x-}, q_{x-}.

As one can see from (76), (77), (78), (79), (80) and (81), the solutions would be travelling waves if both of the following held:

$$\begin{aligned} -s w_- + \theta_{x-} &= 0, \\ s\theta_{x-} - w_- &= 0. \end{aligned}$$

But these hold simultaneously only for $s = \pm 1$ or for $s = \pm c_{\mathrm{m}}$ (cf. (82) and (83)), and $\pm 1, \pm c_{\mathrm{m}}$ are not allowed front speeds. Therefore, we can remove the linear-in-time term from u or from θ and q, but not from all three.

To remove the linear-in-time term from u, one would choose

$$\theta_{x-} = s w_-, \quad \theta_{x+} = s w_+.$$

Since $w_+ > 0$ from (86) and $s w_- < 0$ from (84), the signs of θ_{x+} and θ_{x-} are then determined to be

$$\theta_{x-} < 0, \tag{90}$$

$$s\theta_{x+} > 0. \tag{91}$$

To remove the linear-in-time terms from θ and q instead of u, one would choose

$$\theta_{x-} = \frac{1}{s} w_-, \quad \theta_{x+} = \frac{c_{\mathrm{m}}^2}{s} w_+.$$

The signs of θ_{x-} and θ_{x+} are then given by (90) and (91) in this case, too.

It is not clear whether one should remove the linear-in-time term from u or whether one should remove it from θ and q. Since θ and q are thermodynamic quantities, they are bounded, so one might argue that their linear-in-time terms should be removed. On the other hand, physically unreasonable wind speeds are also undesirable. Perhaps one of $\theta_{x-} = s w_-$ or $\theta_{x-} = w_-/s$ makes more sense than the other based on typical temperature gradients, front speeds, and zonal wind gradients.

Also note that the model variables u, θ, q in (76), (77), (78), (79), (80) and (81) grow linearly in x away from the front. For these precipitation fronts to represent physical solutions on a physical domain, their form would have to be altered away from the dry region–moist region boundary. In this sense the precipitation front solutions (76), (77), (78), (79), (80) and (81) are local solutions in the vicinity of the dry region–moist region boundary, and they might need to be matched with their environment to provide physical solutions. One approach to fitting precipitation fronts on a periodic domain is shown in Fig. 6 of [20]. In that case, there is a discontinuity where two fronts are matched, and gravity waves are initiated from the matching point.

5.2 Numerical solutions

The precipitation front equations (25), (26) and (27) were integrated numerically by FMP using a high order ENO (essentially non-oscillatory) scheme [14]. FMP used a discontinuous initial condition with $\tau_c \neq 0$ in the parameterization for the numerics, and they noted that a continuous precipitation front formed. Looking back at their results, it is clear that the continuous front that formed has the exponential structure found in this paper. Here a continuous precipitation front of the form (76), (77), (78), (79), (80) and (81) will be used initially, and it will evolve just as shown in (76), (77), (78), (79), (80) and (81). This will be confirmed here for a fast moistening front. The parameter values chosen were the same ones used by FMP:

$$\bar{Q} = 0.9, \quad \alpha = 0, \quad \hat{q} = 0.9, \quad \tau_c = 0.25$$

$$s = -2$$

$$w_- = 0.013 \quad w_+ = 0.01$$
$$\theta_{x-} = -0.006 \quad \theta_{x+} = 0$$
$$q_{x-} = 0.00585 \quad q_{x+} = 0$$

The spatial domain in nondimensional units was $-8 < x < 8$; 1,600 grid points were used, so the grid spacing was $\Delta x = 0.01$. The time step used was $\Delta t = 0.00125 = \Delta x/8$ in nondimensional units.

Figure 2 shows the evolution of precipitation P and convergence w. These two quantities are travelling waves. No-flux boundary conditions were used, and this led to waves forming at the boundary and propagating inward. Figure 3 shows the evolution of velocity u, temperature θ, and moisture q. The velocity and temperature plots show that u and θ are not legitimate travelling waves, but q is because $\alpha = 0$ for these numerical solutions.

We plotted these numerical solutions with the exact solutions (76), (77), (78), (79), (80) and (81), and there was no visible difference between the numerical and exact solutions, so we have not shown the comparison here; this comparison confirms the quasi-travelling wave solutions (76), (77), (78), (79), (80) and (81).

To give an idea of the structure of the velocity as a function of x and z, sample vector field plots are shown in Figs. 4 and 5 for each of the three branches of precipitation fronts. These are snapshots in time of the exact solutions (76), (77), (78), (79), (80) and (81) with their full vertical structure from (6) and (7). Figure 4 shows the vector field for a drying front. The parameter values used were

$$\bar{Q} = 0.9, \quad \alpha = 0, \quad \hat{q} = 0.9,$$

$$s = 0.742,$$

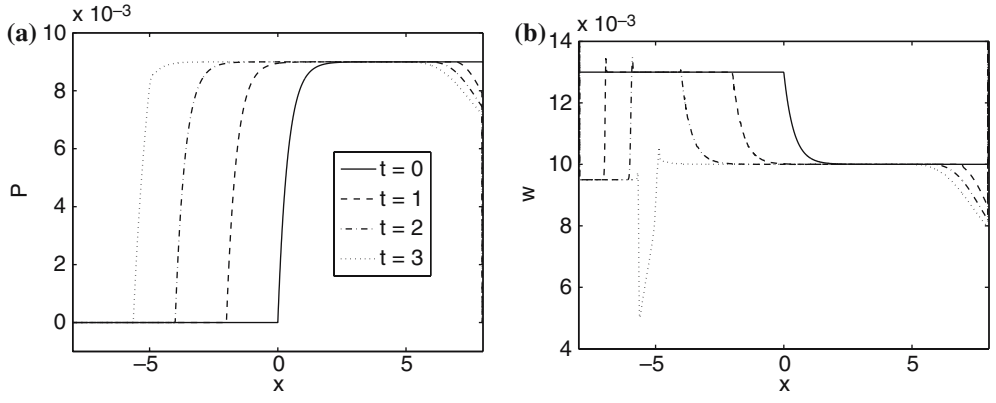

Fig. 2 Numerical travelling wave solutions for a fast moistening front with speed $s = -2$. Four times are shown: $t = 0, 1, 2, 3$. The evolution of precipitation P is shown in **a**, and the the evolution of convergence w is shown in **b**. The no-flux boundary condition leads to a dry gravity wave forming at the left boundary and propagating rightward toward the oncoming precipitation front

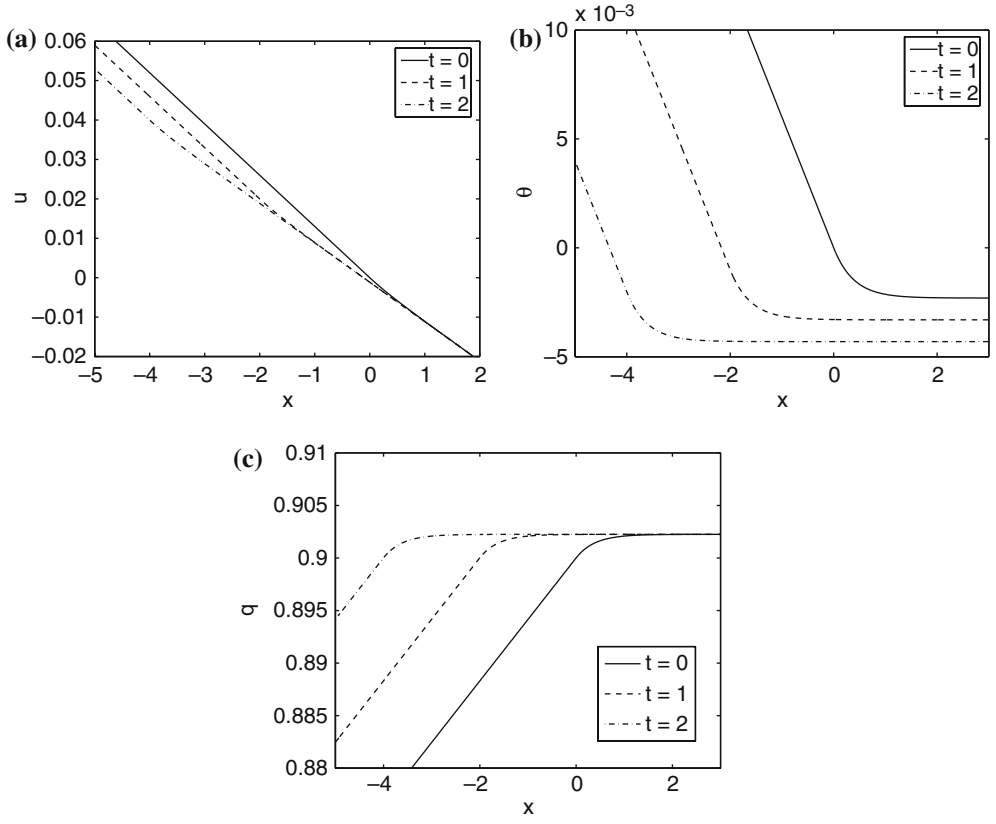

Fig. 3 Numerical travelling wave solutions for a fast moistening front with speed $s = -2$. Three times are shown: $t = 0, 1, 2$. Velocity u is shown in **a**, temperature θ in **b**, and moisture q in **c**. Shortened versions of the full spatial domain $-8 \leq x < 8$ are shown in these plots. Notice that q is the only legitimate travelling wave here, since $\alpha = 0$

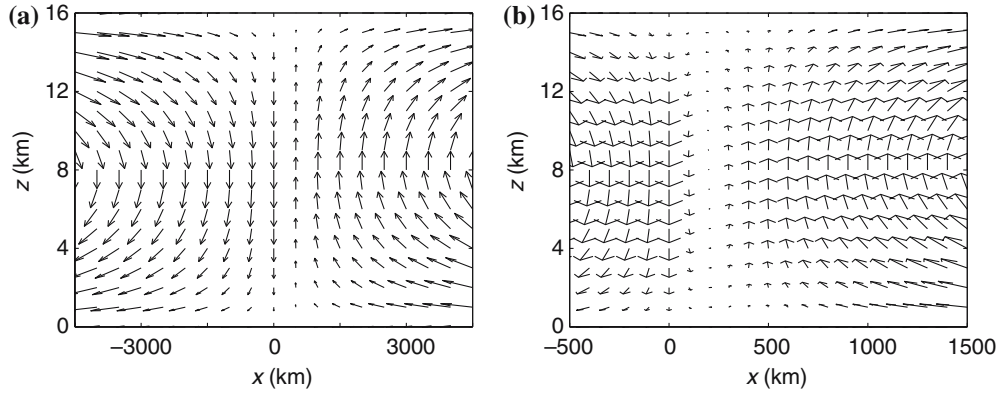

Fig. 4 Velocity field for a drying front for $\tau_c = 2\,\text{h}$ **a**, and a close-up of **a** near the dry region–moist region boundary **b**

$$w_- = -0.01 \quad w_+ = 0.01,$$
$$\theta_{x-} = -0.0148 \quad \theta_{x+} = 0,$$
$$q_{x-} = 0.0121 \quad q_{x+} = 0.$$

(These values were also used by FMP.) Figure 4 uses $\tau_c = 2$ h, and Fig. 4b is a close-up of Fig. 4a near the dry region–moist region boundary. The dry region has large-scale downdrafts and divergence at the surface, and

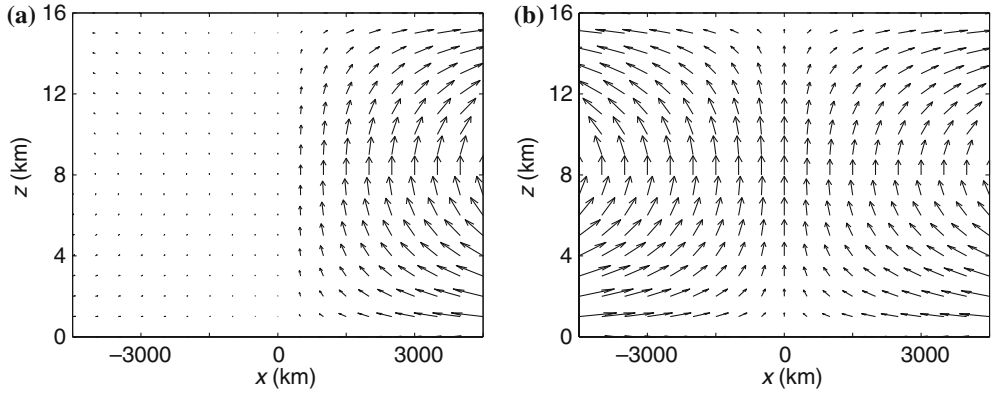

Fig. 5 Velocity field for a slow moistening front **a** and a fast moistening front **b** for $\tau_c = 2$ h

the moist region has large-scale updrafts and convergence at the surface. There is a continuous change from downdrafts to updrafts at $x = 0$ since $\tau_c \neq 0$.

Figure 5a shows the vector field for a slow moistening front. The parameter values used were

$$\bar{Q} = 0.9, \quad \alpha = 0, \quad \hat{q} = 0.9,$$

$$s = -0.158$$

$$\begin{aligned} w_- &= 0.000769 \quad w_+ = 0.01 \\ \theta_{x-} &= 0.00146 \quad \theta_{x+} = 0 \\ q_{x-} &= 0.00438 \quad q_{x+} = 0 \end{aligned}$$

(These values were also used by FMP.) The plot uses $\tau_c = 2$ h. The dry region has large-scale updrafts and convergence at the surface, and the moist region also has large-scale updrafts and convergence at the surface, but the dry region updrafts are less than one-tenth as strong as those in the moist region.

Finally, Fig. 5b shows the vector field for a fast moistening front with $\tau_c = 2$ h. The parameter values used were the ones listed above for the numerical confirmation. Both regions have large-scale updrafts and convergence at the surface, and the updrafts in the dry region are stronger than those in the moist region.

6 Slopes of precipitation fronts and realistic length scales

The length scale τ_c/a determines how steep the front boundary of the solutions (76), (77), (78), (79), (80) and (81) will be. We denote this length scale by L_c:

$$L_c := \frac{\tau_c}{a}. \tag{92}$$

The travelling wave solution for precipitation in the moist region $\tilde{x} > 0$ was given in (66) as

$$P = P_+(1 - e^{-a\tilde{x}/\tau_c}),$$

where P_+ is a positive constant, τ_c is the convective adjustment time from the precipitation parameterization

$$P = \frac{1}{\tau_c}(q - \tilde{q})^+,$$

and a was given in (54) by

$$a = -\frac{1+\alpha}{s}\frac{c_m^2 - s^2}{1 - s^2},$$

where c_m is the moist wave speed,

$$c_{\mathrm{m}} = \sqrt{\frac{1-\bar{Q}}{1+\alpha}}.$$

From this travelling wave form of P and (92), therefore, *the length scale $L_{\mathrm{c}} = \tau_{\mathrm{c}}/a$ determines how steep the precipitation front is*.

In this section, we investigate the dependence of L_{c} on the parameters τ_{c}, $\bar{Q}$, α, and s, and we consider the physical significance of the parameters' effects.

As mentioned earlier near (24), values for the parameters $\bar{Q}$ and α will be chosen so that $c_{\mathrm{m}} \approx 15\,\mathrm{m/s}$, in agreement with the observations of Wheeler and Kiladis [42]. For $0 < \alpha < 1$, $\bar{Q}$ is typically chosen to be close to 0.8 or 0.9. These choices lead to moist wave speeds near the observed value of 15 m/s. Table 3 shows the moist wave speed c_{m} resulting from some combinations of $\bar{Q}$ and α. The choices of $\bar{Q}$ we will consider are 0.8, 0.9, and 0.95. The value 0.95 is chosen mainly as a comparison for the smaller values of 0.8 and 0.9. The choices of α we will consider are –0.3, 0, 0.5, 1, and 1.5. The choice –0.3 appears to be nonphysical, since potentially warm air can hold more moisture than cold air; we include it to get an idea of the consequences of the entire range of allowed α values, $\alpha > -\bar{Q}$.

We now consider the effect of these parameters on the steepness of the front in detail, and we show some plots to make the dependencies clearer.

Dependence of L_{c} on τ_{c} Of the four parameters τ_{c}, $\bar{Q}$, α, and s, it is easiest to see how L_{c} depends on τ_{c}, since it is a linear relationship. Figure 6a shows what the precipitation would look like for two common values of τ_{c}: 2 and 12 h. The other parameter values chosen were $\bar{Q} = 0.9$, $\alpha = 0$, and $s = -4\,\mathrm{m/s}$. The plot shows that the front with $\tau_{\mathrm{c}} = 12\,\mathrm{h}$ is probably too broad to be physically reasonable, since the front requires approximately 6,000 km to get within 95% of its asymptotic value. In fact, the front with $\tau_{\mathrm{c}} = 2\,\mathrm{h}$ might also be a little broad in this case, since the front takes about 1,500 km to reach 95% of its asymptotic value.

One should *not* conclude from this discussion that $\tau_{\mathrm{c}} = 12\,\mathrm{h}$ always leads to fronts with physically unreasonable slopes. One may, though, conclude that $\tau_{\mathrm{c}} = 12\,\mathrm{h}$ leads to fronts with physically reasonable slopes *for a smaller range of s* than $\tau_{\mathrm{c}} = 2\,\mathrm{h}$ does. For instance, Figure 6b shows the fronts for $\tau_{\mathrm{c}} = 2$ and 12 h when a moistening front of speed $s = -1\,\mathrm{m/s}$ is chosen instead. In this case, both values of τ_{c} lead to fronts with physically reasonable slopes.

Table 3 Moist wave speed c_{m} in metre per second for three values of $\bar{Q}$ and five values of α. Observational studies show 15 m/s as a typical moist wave speed.

		α				
		–0.3	0	0.5	1	1.5
$\bar{Q}$	0.8	27	22	18	16	14
	0.9	19	16	13	11	10
	0.95	13	11	9	8	7

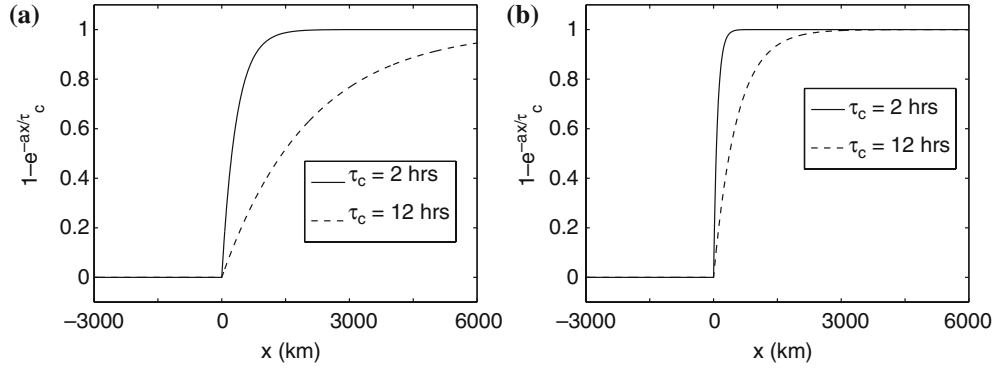

Fig. 6 **a** A precipitation front for two values of τ_{c}: 2 and 12 h. The other parameter values chosen were $\bar{Q} = 0.9$, $\alpha = 0$, and $s = -4\,\mathrm{m/s}$. **b** A precipitation front for two values of τ_{c}: 2 and 12 h. Whereas plot **a** used $s = -4\,\mathrm{m/s}$, plot **b** uses $s = -1\,\mathrm{m/s}$. Both front profiles in plot **b** seem physically reasonable

We will define a front profile as "physically reasonable" if 95% of its asymptotic moist value is reached by 1,500 km (the dry/moist region boundary is at $x = 0$). This corresponds to

$$0 \le L_c \le 500\,\text{km},$$

or

$$0 \le L_c \le 1/3$$

in nondimensional units. The physically reasonable front speeds will then be a subset of the allowed front speeds in (57), (58) and (59), and in the limit $\tau_c \to 0$, the physically reasonable front speeds are the same as the allowed front speeds.

Figure 7a shows front profiles for several values of L_c. As an example, the physically reasonable front speeds for $\alpha = 0$, $\bar{Q} = 0.9$ are

$$\begin{aligned} &30\ \text{m/s} < s < 50\ \text{m/s}, \\ &-6\ \text{m/s} < s < 0\ \text{m/s} \quad \text{for} \quad \tau_c = 2\ \text{h} \\ &-90\ \text{m/s} < s < -50\ \text{m/s} \end{aligned}$$

and

$$\begin{aligned} &45\ \text{m/s} < s < 50\ \text{m/s} \\ &-1\ \text{m/s} < s < 0\ \text{m/s} \quad \text{for} \quad \tau_c = 12\ \text{h} \\ &-55\ \text{m/s} < s < -50\ \text{m/s}. \end{aligned}$$

When $\tau_c = 12\,\text{h}$ is used, the range of physically reasonable front speeds is significantly smaller than it is for $\tau_c = 2\,\text{h}$.

For fixed s, although the front's physical structure changes as τ_c decreases, the front of speed s will always be a realizable solution for any value of $\tau_c \ge 0$. Therefore, the strict quasi-equilibrium limit $\tau_c \to 0$ is useful for prediciting propagation speeds of precipitating regions, even if no information of the physical structure of the front survives in the limit.

In short, smaller τ_c values lead to steeper fronts and wider ranges of physically reasonable front speeds. As we shall see below, $\bar{Q}$ and α will also affect the physically reasonable front speeds but in a more complicated way. In the rest of the plots in this section, the value $\tau_c = 2\,\text{h}$ will be used.

Dependence of L_c on s. The front velocity s appears in three places in L_c:

$$L_c = -\tau_c \frac{s}{1+\alpha} \frac{1-s^2}{c_m^2 - s^2}.$$

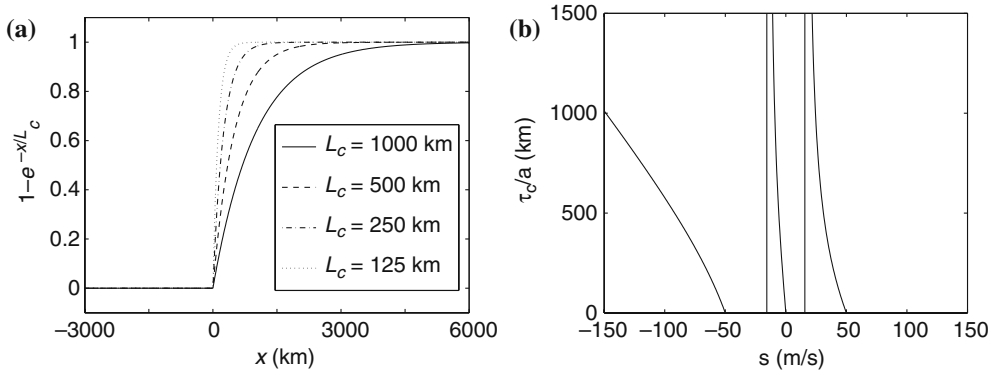

Fig. 7 **a** Front profiles for four different values of L_c: 1,000, 500, 250, and 125 km. Each branch of fronts has a front with each of these profiles. Fronts for which $0 \le L_c \le 500\,\text{km}$ are called "physically reasonable." **b** Plot of $L_c = \tau_c/a$ versus s for $\alpha = 0$, $\bar{Q} = 0.9$, and $\tau_c = 2\,\text{h}$. *Vertical lines* denote $s = \pm c_m$

Figure 7b shows L_c versus s. For all three branches of fronts, L_c decreases as s increases; that is, the front steepens as s increases. The steepest fast moistening fronts have speeds near −50 m/s, the steepest slow moistening fronts have speeds near 0 m/s, and the steepest drying fronts have speeds near +50 m/s.

To get an idea of what a front of a certain speed looks like, the left plot of Fig. 7a shows front profiles for L_c =1,000, 500, 250, and 125 km. For $\bar{Q} = 0.9$, $\alpha = 0$, and $\tau_c = 2$ h, these profiles correspond to fronts with the following speeds:

L_c (km)	s (m/s)		
1,000	+24	−9.4	−150
500	+31	−6.0	−94
250	+38	−3.3	−69
125	+43	−1.7	−59

As discussed above, using different parameter values, such as τ_c, can change these front slopes dramatically.

Dependence of L_c on $\bar{Q}$ The parameter $\bar{Q}$ affects the moist wave speed significantly, as was shown in Table 3, and it is through this dependence that $\bar{Q}$ affects L_c. Its effect is through the term $c_m^2 - s^2$ of a.

Figure 8a shows example plots of precipitation for $\alpha = 0$, $s = 35$ m/s. The front becomes steeper as $\bar{Q}$ increases. This is also the case for fast moistening fronts, but the opposite is true for slow moistening fronts.

In the rest of the plots in this section, the value $\bar{Q} = 0.9$ will be used.

Dependence of L_c on α. Increasing α decreases c_m, which affects L_c through the term $c_m^2 - s^2$. There is also a $1 + \alpha$ term of L_c. As was the case with $\bar{Q}$, α affects L_c in different ways for different fronts. Figure 8b shows a precipitation profile for varying α. This is a drying front for $s = 35$ m/s, and the front steepens for increasing α. This is also the case for fast moistening fronts, whereas increasing α broadens slow moistening fronts.

7 Summary

Exact analytical precipitation front solutions were found for a simplified tropical climate model. The model includes two vertical modes – a barotropic mode and the first baroclinic mode – and precipitation is parameterized by a Betts–Miller scheme with a finite relaxation time. The precipitation fronts come in three types: drying fronts, slow moistening fronts, and fast moistening fronts. The exact precipitation front solutions hold for finite convective adjustment times ($\tau_c \neq 0$), thus demonstrating robust realizability of all three types of fronts, even though the moistening fronts violate Lax's stability criterion.

As a study of the waves supported by a convective parameterization, these precipitation fronts provide some physically appealing solutions and some solutions that appear unphysical. The slow moistening fronts are appealing, since large-scale regions of precipitation travelling at roughly 5 m/s are present in the tropics. Fast moistening fronts, though, can travel at arbitrarily high speeds; and, as shown in Sect. 6, some fronts

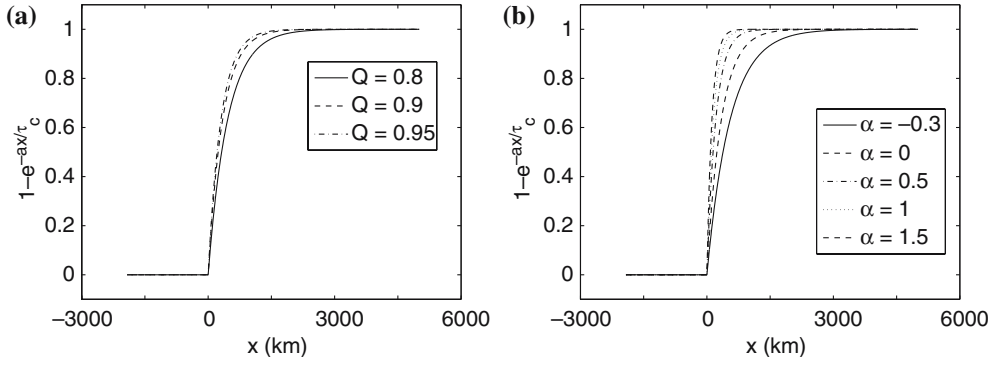

Fig. 8 **a** A precipitation front for three values of $\bar{Q}$: 0.8, 0.9, and 0.95. This is a drying front with $\alpha = 0$, $s = 35$ m/s. Fast moistening fronts also show this trend (i.e., they steepen as $\bar{Q}$ increases), whereas slow moistening fronts broaden as $\bar{Q}$ increases. **b** A precipitation front for five values of α: –0.3, 0, 0.5, 1, and 1.5. This is a drying front with speed 35 m/s. The drying front steepens as α increases. Fast moistening fronts also show this trend, whereas slow moistening fronts broaden as α increases

of all three types are so broad that they can hardly be considered as fronts. The parameterization considered here, along with the simplified tropical climate model in which it is used, thus supports a wide variety of precipitation fronts.

The precipitation fronts found here for finite relaxation times τ_c have the same front speeds as the discontinuous fronts of FMP. Although a front's steepness depends on τ_c, a front with front velocity s is always realizable for any $\tau_c \geq 0$. Thus the strict quasi-equilibrium limit $\tau_c \to 0$ is useful for predicting propagation speeds of precipitating regions, even if the front is not nearly discontinuous.

From the viewpoint of applied mathematics, exact analytic solutions were found to the remarkable new system of partial differential equations1 (9), (10), (11), (12) and (13), a simplified tropical climate model. See FMP for a list of several interesting problems for applied analysis with this model, and see [19–22,37] for more geophysical results with this model.

Appendix A Calculating solutions to the derivative equations

Integrating the ODE (53) for Z_x then gives

$$Z_x = C_z \exp\left(\frac{1+\alpha}{s}\frac{c_m^2 - s^2}{1-s^2}\left[\frac{x-st}{\tau_c}\right]\right) + \frac{\bar{Q}+\alpha}{1+\alpha}\frac{1-s^2}{c_m^2-s^2}C_\theta.$$

Using (43) and (51) and (52) the variables w, θ_x, q_x are then

$$\begin{aligned} w = {} & \frac{C_z}{1-\bar{Q}}\frac{s}{1-s^2}\exp\left(\frac{1+\alpha}{s}\frac{c_m^2-s^2}{1-s^2}\left[\frac{x-st}{\tau_c}\right]\right) \\ & + \frac{s}{1-\bar{Q}}\frac{\bar{Q}+\alpha}{1+\alpha}\frac{1}{c_m^2-s^2}C_\theta + C_w \end{aligned} \tag{93}$$

$$\theta_x = \frac{C_z}{1-\bar{Q}}\frac{s^2}{1-s^2}\exp\left(\frac{1+\alpha}{s}\frac{c_m^2-s^2}{1-s^2}\left[\frac{x-st}{\tau_c}\right]\right) + \frac{1}{1+\alpha}\frac{1-s^2}{c_m^2-s^2}C_\theta \tag{94}$$

$$q_x = \frac{C_z}{1-\bar{Q}}\frac{1-\bar{Q}-s^2}{1-s^2}\exp\left(\frac{1+\alpha}{s}\frac{c_m^2-s^2}{1-s^2}\left[\frac{x-st}{\tau_c}\right]\right) + \frac{\alpha}{1+\alpha}\frac{1-s^2}{c_m^2-s^2}C_\theta. \tag{95}$$

There are three unknown constants of integration here: C_w, C_θ, C_z. These constants are found be requiring these moist region solutions (93), (94) and (95) to match the dry region solutions (38)–(40) at the boundary $\tilde{x} = 0$. The result is a linear system of equations for the constants C_w, C_θ, C_z. Since it is straightforward but messy to solve the linear system, the details are omitted here. Inserting the values of C_w, C_θ, C_z into (93), (94) and (95) leads to the moist region solutions:

$$\begin{aligned} w &= w_+ - [w]\mathrm{e}^{-a\tilde{x}/\tau_c} \\ \theta_x &= \theta_{x+} - [\theta_x]\mathrm{e}^{-a\tilde{x}/\tau_c} \\ q_x &= q_{x+} - [q_x]\mathrm{e}^{-a\tilde{x}/\tau_c}, \end{aligned}$$

where a was given in (54) as

$$a = -\frac{1+\alpha}{s}\frac{c_m^2-s^2}{1-s^2},$$

and c_m is the moist wave speed, given in (24) as

$$c_m = \sqrt{\frac{1-\bar{Q}}{1+\alpha}}.$$

The parameters w_+, θ_{x+}, q_{x+} are the moist region counterparts to w_-, θ_{x-}, q_{x-}, and they are given by

$$w_+ := \lim_{\tilde{x}\to+\infty} w = -\frac{1}{1+\alpha}\frac{s}{c_{\mathrm{m}}^2 - s^2}(q_{x-} - \alpha\theta_{x-}) + w_-, \tag{96}$$

$$\theta_{x+} := \lim_{\tilde{x}\to+\infty} \theta_x = -\frac{1}{1+\alpha}\frac{s^2}{c_{\mathrm{m}}^2 - s^2}(q_{x-} - \alpha\theta_{x-}) + \theta_{x-}, \tag{97}$$

$$q_{x+} := \lim_{\tilde{x}\to+\infty} q_x = -\frac{\alpha}{1+\alpha}\frac{s^2}{c_{\mathrm{m}}^2 - s^2}(q_{x-} - \alpha\theta_{x-}) + \alpha\theta_{x-}. \tag{98}$$

They could have been obtained alternatively by taking the limit $\tau_{\mathrm{c}} \to 0$ instead of $\tilde{x} \to +\infty$. The asymptotic jump in the variables across the front is given by

$$\begin{aligned}
[w] &= w_+ - w_-, \\
[\theta_x] &= \theta_{x+} - \theta_{x-}, \\
[q_x] &= q_{x+} - q_{x-}.
\end{aligned}$$

From these definitions, one immediately sees that

$$s[w] = [\theta_x], \tag{99}$$

$$q_{x+} = \alpha\theta_{x+}, \tag{100}$$

$$[q_x] = \left(\frac{1-\bar{Q}}{s} - s\right)[w]. \tag{101}$$

Appendix B Integrating the solutions to the derivative equations

To find ODEs for the functions f_u, f_θ, f_q, insert the formulas (70), (71) and (72) for the dry region solutions into the model equations (25), (26) and (27). The dry region functions f_u, f_θ, f_q must then satisfy:

$$\frac{\mathrm{d}f_u}{\mathrm{d}t} = \theta_{x-} - sw_-, \tag{102}$$

$$\frac{\mathrm{d}f_\theta}{\mathrm{d}t} = s\theta_{x-} - w_-, \tag{103}$$

$$\frac{\mathrm{d}f_q}{\mathrm{d}t} = sq_{x-} + \bar{Q}w_-. \tag{104}$$

Integrating these gives

$$\begin{aligned}
f_u(t) &= (\theta_{x-} - sw_-)t + u(0,0), \\
f_\theta(t) &= (s\theta_{x-} - w_-)t + \theta(0,0), \\
f_q(t) &= (sq_{x-} + \bar{Q}w_-)t + \hat{q} + \alpha\theta(0,0),
\end{aligned}$$

where $u(0,0)$ is the velocity at $x = t = 0$. The constants of integration have been chosen to make later calculations easier.

The same procedure is done for g_u, g_θ, g_q, and the result is

$$\begin{aligned}
g_u(t) &= (\theta_{x+} - sw_+)t + \frac{\tau_{\mathrm{c}}}{a}[w] + u(0,0) \\
g_\theta(t) &= (s\theta_{x+} - w_+ + P_+)t - \frac{\tau_{\mathrm{c}}}{a}[\theta_x] + \theta(0,0) \\
g_q(t) &= (sq_{x+} + \bar{Q}w_+ - P_+)t - \frac{\tau_{\mathrm{c}}}{a}[q_x] + \hat{q} + \alpha\theta(0,0),
\end{aligned}$$

where the constants of integration have been chosen to make later calculations easier.

The six functions of time $g_u, g_\theta, g_q, f_u, f_\theta, f_q$ have now been determined, but continuity constraints still must be met. First note that precipitation will be continuous if $\hat{q} = q(0) - \alpha\theta(0)$. From (70), (71) and (72) and from (73), (74) and (75), this is satisfied if

$$f_q(t) = \hat{q} + \alpha f_\theta(t), \tag{105}$$

$$g_q(t) = \hat{q} + \alpha g_\theta(t) + \frac{\tau_c}{a}(q_{x-} - \alpha\theta_{x-}). \tag{106}$$

From the solutions for the fs and gs above, these constraints lead to

$$s = -\frac{\bar{Q} + \alpha}{q_{x-} - \alpha\theta_{x-}} w_-, \tag{107}$$

$$P_+ = \frac{\bar{Q} + \alpha}{1 + \alpha} w_+. \tag{108}$$

Also, there are three more continuity constraints. To have continuous u, θ, and q, the dry and moist region solutions must match at $\tilde{x} = 0$. Therefore

$$g_u(t) = f_u(t) + \frac{\tau_c}{a}[w], \tag{109}$$

$$g_\theta(t) = f_\theta(t) - \frac{\tau_c}{a}[\theta_x], \tag{110}$$

$$g_q(t) = f_q(t) - \frac{\tau_c}{a}[q_x]. \tag{111}$$

One can see that these constraints (105), (106) and (109), (110) and (111) are met by the fs and gs found above by using the relations (63), (64) and (65), (67), (68), and (107) and (108); and one can see why the constants of integration in the fs and gs were chosen as they were.

Acknowledgements The authors thank Olivier Pauluis and Dargan Frierson for helpful discussion. Comments from two anonymous reviewers also helped improve the manuscript. Samuel Stechmann is supported by a Department of Energy Computational Science Graduate Fellowship under grant number DE–FG02–97ER25308. The research of Andrew Majda is partially supported by a grant from the Office of Naval Research, ONR # N00014–96–1–0043, and two National Science Foundation grants, NSF # DMS–96225795 and NSF–FRG # DMS–0139918.

References

1. Arakawa, A., Schubert, W.H.: Interaction of a cumulus cloud ensemble with the large-scale environment, Part I. J. Atmos. Sci. **31**, 674–701 (1974)
2. Betts, A.K., Miller, M.J.: A new convective adjustment scheme. Part II: Single column tests using GATE wave, BOMEX, and arctic airmass data sets. Q. J. R. Meteor. Soc. **112**, 693–709 (1986)
3. Bourlioux, A., Majda, A.J.: Theoretical and numerical structure of unstable detonations. Philos. Trans. R. Soc. Lond. A **350**, 29–68 (1995)
4. Bretherton, C.S., Peters, M.E., Back, L.E.: Relationships between water vapor path and precipitation over the tropical oceans. J. Clim. **15**, 2907–2920 (2004)
5. Chen, G.Q., Levermore, C.D., Liu, T.P.: Hyperbolic conservation laws with stiff relaxation terms and entropy. Commun. Pure Appl. Math. **47**(6), 787–830 (1994)
6. Colella, P., Majda, A., Roytburd, V.: Theoretical and numerical structure for reacting shock waves. SIAM J. Sci. Stat. Comput. **7**(4), 1059–1080 (1986)
7. Emanuel, K.A.: An air–sea interaction model of intraseasonal oscillations in the tropics. J. Atmos. Sci. **44**, 2324–2340 (1987)
8. Emanuel, K.A.: Atmospheric convection. Oxford University Press, London (1994)
9. Emanuel, K.A., Neelin, J.D., Bretherton, C.S.: On large-scale circulations in convecting atmospheres. Q. J. R. Meteor. Soc. **120**(519), 1111–1143 (1994)
10. Folland, G.B.: Introduction to partial differential equations. Princeton University Press, Princeton, (1976)
11. Frierson, D.M.W., Majda, A.J., Pauluis, O.M.: Large scale dynamics of precipitation fronts in the tropical atmosphere: a novel relaxation limit. Commun. Math. Sci. **2**(4), 591–626 (2004)
12. Fuchs, E., Raymond, D.J.: Large-Scale Modes of a Nonrotating Atmosphere with water vapor and cloud-radiation feedbacks. J. Atmos. Sci. **59**, 1669–1679 (2002)
13. Gill, A.E.: Atmosphere–ocean dynamics, International Geophysics Series, vol. 30. Academic, New York, (1986)
14. Harten, A., Engquist, B., Osher, S., Chakravarthy, S.R.: Uniformly high-order accurate essentially nonoscillatory schemes. III. J. Comput. Phys. **71**(2), 231–303 (1987)
15. James, I.N.: Introduction to circulating atmospheres. Cambridge Atmospheric and Space Science Series. Cambridge University Press, London, (1995)

16. Jin, S., Xin, Z.P.: The relaxation schemes for systems of conservation laws in arbitrary space dimensions. Commun. Pure Appl. Math. **48**(3), 235–276 (1995)
17. Johnson, R.H., Rickenbach, T.M., Rutledge, S.A., Ciesielski, P.E., Schubert, W.H.: Trimodal characteristics of tropical convection. J. Atmos. Sci. **12**, 2397–2418 (1999)
18. Katsoulakis, M.A., Tzavaras, A.E.: Contractive relaxation systems and the scalar multidimensional conservation law. Commun. Part. Diff. Eqns. **22**(1-2), 195–233 (1997)
19. Khouider, B., Majda, A.J.: A non-oscillatory balanced scheme for an idealized tropical climate model: Part I: algorithm and validation. Theor. Comp. Fluid Dyn. **19**(5), 331–354 (2005)
20. Khouider, B., Majda, A.J.: A non-oscillatory balanced scheme for an idealized tropical climate model: Part II: nonlinear coupling and moisture effects. Theor. Comp. Fluid Dyn. **19**(5), 355–375 (2005)
21. Khouider, B., Majda, A.J.: A simple multicloud parameterization for convectively coupled tropical waves. Part I: linear analysis. J. Atmos. Sci. **63**, 1308–1323 (2006)
22. Khouider, B., Majda, A.J.: A simple multicloud parameterization for convectively coupled tropical waves. Part II: Nonlinear simulations. J. Atmos. Sci. (2006, in press)
23. Lax, P.D.: Hyperbolic systems of conservation laws. II. Commun. Pure Appl. Math. **10**, 537–566 (1957)
24. Madden, R.A., Julian, P.R.: Observations of the 40–50-day tropical oscillation – a review. Mon. Wea. Rev. **122**, 814–837 (1994)
25. Majda, A.: A qualitative model for dynamic combustion. SIAM J. Appl. Math. **41**(1), 70–93 (1981)
26. Majda, A.: Compressible fluid flow and systems of conservation laws in several space variables, Applied Mathematical Sciences, vol. 53. Springer, Berlin Heidelberg New York, (1984)
27. Majda, A.: Introduction to PDEs and waves for the atmosphere and ocean, Courant Lecture Notes in Mathematics, vol. 9. New York University Courant Institute of Mathematical Sciences, New York, (2003)
28. Majda, A.J., Khouider, B., Kiladis, G.N., Straub, K.H., Shefter, M.G.: A model for convectively coupled tropical waves: nonlinearity, rotation, and comparison with observations. J. Atmos. Sci. **61**, 2188–2205 (2004)
29. Majda, A.J., Shefter, M.G.: Models of stratiform instability and convectively coupled waves. J. Atmos. Sci. **58**, 1567–1584 (2001)
30. Majda, A.J., Shefter, M.G.: Waves and instabilities for model tropical convective parameterizations. J. Atmos. Sci. **58**, 896–914 (2001)
31. Moncrieff, M.W., Klinker, E.: Organized convective systems in the tropical western pacific as a process in general circulation models: a toga coare case-study. Q. J. R. Meteor. Soc. **123**(540), 805–827 (1997)
32. Nakazawa, T.: Tropical super clusters within intraseasonal variations over the western pacific. J. Meteor. Soc. Jpn. **66**(6), 823–839 (1988)
33. Neelin, J.D., Held, I.M.: Modeling tropical convergence based on the moist static energy budget. Mon. Wea. Rev. **115**, 3–12 (1987)
34. Neelin, J.D., Held, I.M., Cook, K.H.: Evaporation–wind feedback and low-frequency variability in the tropical atmosphere. J. Atmos. Sci. **44**, 2341–2348 (1987)
35. Neelin, J.D., Yu, J.Y.: Modes of tropical variability under convective adjustment and the madden–julian oscillation. Part 1: analytical theory. J. Atmos. Sci. **51**, 1876–1894 (1994)
36. Neelin, J.D., Zeng, N.: A quasi-equilibrium tropical circulation model — formulation. J. Atmos. Sci. **57**, 1741–1766 (2000)
37. Pauluis, O., Majda, A.J., Frierson, D.M.W.: Propagation, reflection, and transmission of precipitation fronts in the tropical atmosphere. (in preparation) (2006)
38. Philander, S.G.: El Niño, La Niña, and the Southern Oscillation. International Geophysics Series. Academic, New York, (1989)
39. Slingo, J.M., et al.: Intraseasonal oscillations in 15 atmospheric general circulation models: results from an amip diagnostic subproject. Clim. Dyn. **12**(5), 325–357 (1996)
40. Smith, R.K. (ed.): The physics and parameterization of moist atmospheric convection. NATO Science Series C: Mathematical and Physical Sciences. Kluwer, Dordrecht, (2004)
41. Straub, K.H., Kiladis, G.N.: Observations of a convectively coupled kelvin wave in the eastern pacific itcz. J. Atmos. Sci. **59**, 30–53 (2002)
42. Wheeler, M., Kiladis, G.N.: Convectively coupled equatorial waves: analysis of clouds and temperature in the wavenumber–frequency domain. J. Atmos. Sci. **56**(3), 374–399 (1999)
43. Wheeler, M., Kiladis, G.N., Webster, P.J.: Large-scale dynamical fields associated with convectively coupled equatorial waves. J. Atmos. Sci. **57**(5), 613–640 (2000)
44. Williams, F.A.: Combustion theory. Addison Wesley, Reading, (1985)
45. Yano, J.I., Emanuel, K.A.: An improved model of the equatorial troposphere and its coupling to the stratosphere. J. Atmos. Sci. **48**, 377–389 (1991)
46. Yano, J.I., McWilliams, J.C., Moncrieff, M.W., Emanuel, K.A.: Hierarchical tropical cloud systems in an analog shallow-water model. J. Atmos. Sci. **52**, 1723–1742 (1995)